

東京大学 大学院新領域創成科学研究科
基盤科学研究系
先端エネルギー工学専攻

平成 22 年度

修士論文

Light-Weight Flexible Rectenna for

Wireless Power Transmission to Flying Objects

— 飛行体への無線電力伝送における軽量フレキシブルレクテナ —

2011 年 2 月提出

指導教員 小紫 公也 教授

96069 澤原 弘憲

Preface

This paper reports development of the light-weight flexible patch rectenna for the receiving system. I designed and fabricated antennas, RF-DC conversion circuits, and rectennas, and measured their power conversion efficiencies. As a result the antennas were developed with the average polarized wave efficiency of 70% and the return loss efficiency of 99%. The RF-DC conversion circuits were also developed with the conversion efficiency of maximum 58% at 65mW and 100 Ω load resistance. Until this development, there were no high efficiency and light-weight flexible rectenna. Therefore, the rectennas are very useful for Micro Aerial Vehicles and so on. Moreover, I produced a rectenna array consisted of ten rectenna elements in parallel, and succeeded to operate the electric motor for MAV model and demonstrate the MAV.

I would like to express my sincere appreciation to Professor Kimiya Komurasaki, Department of Advanced Energy, University of Tokyo, for many valuable discussions, suggestions, supports and encouragements. I'm grateful to express my thanks to Professor Yoshihiro Arakawa, Department of Aeronautics and Astronautics, University of Tokyo, for his advice and discussion. Thanks also to Mr. Oda, Ms. Ishiba, Mr. Ishida and Mr. Miyashiro who are Microwave Power Transmission Research Group for the helping in the experiments. I would like to thank Associate Professor Koji Tanaka (Institute of Space and Astronautical Science: ISAS, Japan Aerospace Exploration Agency: JAXA) for his advice about the microwave power transmission and the experiment. I'm obliged to all the member of Komurasaki lab and Arakawa lab, especially Messrs. Satoshi Nomura, Mr. Koizumi and Mr. Mizuno for helping my research. Without any of these supports, this thesis would not have been completed. Thank you so much.

Finally, I would like to my special appreciation to my parents for their financial and mental support throughout my education.

February, 2011

Hironori Sawahara

Contents

List of figures	IV
List of tables	VII
Chapter 1 Introduction	1
1.1 Wireless Power Transmission	1
1.2 Microwave Wireless Power Transmission	3
1.3 MWPT to Micro Aerial Vehicle and Purpose of the thesis	5
Chapter 2 Basic Theory	7
2.1 Wave Propagation and Polarization	7
2.1.1 Linear polarized wave	7
2.1.2 Circular polarized wave	9
2.1.3 Polarization Choice for MAV	10
2.2 Transmission Line Theory	11
2.2.1 Wave Propagation on a Transmission Line	11
2.2.2 The Lossless Line	13
2.2.3 The Terminated Lossless Transmission Line	14
Chapter 3 Theories of Rectenna elements	15
3.1 Theory of Rectenna Design	15

3.2	Theory of Antenna Design	17
3.2.1	Size Designing of MSA	17
3.2.2	Impedance Matching Method between MSA element and Feeding System	17
3.2.3	Interior Electromagnetic Field of Rectangular MSA	19
3.2.4	Methods for Polarity-free Antenna	23
3.3	Theory of Rectifier Circuit Design	25
3.3.1	Rectifier Circuit Model in Lumped Parameter System	26
3.3.2	Matching of Input Impedance	28
3.3.3	Design of Stub	29
3.3.4	Output load-line Characteristics	30
3.3.5	Rectifier Circuit Model in Distributed Parameter System	32

Chapter 4 Experimental Apparatus 33

4.1	Power Transmission System	33
4.1.1	Oscillator	35
4.1.2	Power divider	36
4.1.3	6-bit digital phase shifter	37
4.1.4	Driver amplifier	38
4.1.5	Power amplifier	39
4.1.6	Booster amplifier	40
4.1.7	Horn antenna	41
4.1.8	Circularizer	42
4.2	Power Receiving System / Measurement Apparatus	43
4.2.1	Light-Weight Flexible Patch Antenna / Rectenna	44
4.2.2	Power Sensor and Power Meter	46
4.2.3	Adjustable Resistor	47
4.2.4	Digital Multi Meter	48
4.2.5	Signal Generator	48
4.2.6	Network Analyzer	49
4.3	Experimental Setup and Demonstration	50
4.3.1	Mounting structure	50
4.3.2	Electrical Motor for MAV Model	51
4.3.3	MAV Model and Demonstration	52

Chapter 5	Measurement Results and Discussions	54
5.1	Antenna Measurement	54
5.1.1	Dielectric Constant	54
5.1.2	Dependence of Yaw-Angle	56
5.1.3	Characteristic of Antenna (Return Loss)	57
5.2	RF-DC Conversion Circuit Measurement	59
5.2.1	Capacitance of Chip Condenser: C_0	61
5.2.2	Length of Diode and Ground: l_g	62
5.2.3	Pieces Number of the Low Pass Filter	63
5.2.4	Input Line Width: W	64
5.2.5	Diode Variations: D	65
5.2.6	Redesign of Rectifier Circuit	66
5.2.7	Bending Properties	67
5.2.8	Dependence of Input Power	68
5.3	Rectenna Array Measurement	69
5.3.1	Optimization of Array Pitch	69
5.3.2	Two Antenna Elements for One Rectifier Circuit	70
5.4	MAV Model Demonstration	72
5.4.1	Parallel Connection of Rectenna	72
5.4.2	Total Efficiency in Receiving System	73
5.4.3	MAV Model Demonstration	74
Chapter 6	Conclusions	75
6.1	Conclusions	75
6.2	Future Perspectives and Issues	76
References		77
Accomplishments		79

List of figures

Figure 1.1 Classification of Wireless Power Transmission	1
Figure 1.2 Experiment of MWPT to a helicopter	4
Figure 1.3 Schematic of the MAV system	6
Figure 2.1 Schematic of Planar wave (TEM) Propagation	8
Figure 2.2 Schematic of Rotating Polarization Plane	9
Figure 2.3 Voltage and current definitions and equivalent circuit	12
Figure 2.4 A transmission line terminated in a load impedance Z_L	14
Figure 3.1a Schematic of Rectenna	16
Figure 3.1b RF-DC Conversion Efficiency of Rectenna	16
Figure 3.2 Feeding Methods of MSA Element	18
Figure 3.3 Rectangular MSA and its Coordinate System	19
Figure 3.4 Schematic of Electromagnetic Distribution of TM ₁₀₀ wave	22
Figure 3.5 Pattern of Unit of Multiple Dipole Antenna	23
Figure 3.6 Pattern of Patch Antenna for Circular Polarized Wave	24
Figure 3.7 Simple Schematic of Rectifier Circuit with Input and Output Filters	25
Figure 3.8 Schematic of Rectifier Circuit with Lumped-element Input and Output Filters	26
Figure 3.9 Schematic of Rectifier Circuit with a Transmission Line as Output Filter	26
Figure 3.10 Rectifier Circuit Pattern	27
Figure 3.11 Schematic of Rectifier Circuit for Experiment	27
Figure 3.12 Structure of Micro-Strip Line	28
Figure 3.13 Pattern and Equivalent Circuit of Micro-Strip Stub	29
Figure 3.14 Relationship between DC equivalent circuit and load-line	30
Figure 3.15 V-I Characteristic of Diode	31
Figure 3.16 Equivalent Circuit of Diode	32
Figure 3.17 Detailed Schematic of Rectifier Circuit for Experiment	32
Figure 4.1 Schematic of Transmitting Array antenna System	33

Figure 4.2 Picture of Transmitting System (1: Power Amplifiers, 2: Driver Amplifiers,3: Phase Shifters, 4: Booster Amplifier, 5: Oscillator, 6: 8 Power Divider, 7: Power Source)	34
Figure 4.3 Arrangement of five antenna elements of the array	34
Figure 4.4 Picture of Oscillator	35
Figure 4.5 Picture of Power Divider	36
Figure 4.6 Picture of Phase Shifter	37
Figure 4.7 Mechanism of phase shifting	37
Figure 4.8 Picture of Driver Amplifier	38
Figure 4.9 Picture of Power Amplifier	39
Figure 4.10 Picture of Booster Amplifier	40
Figure 4.11 Picture of Horn-Antenna	41
Figure 4.12 Picture of Circularizer	42
Figure 4.13 Schematic of Power Receiving System	43
Figure 4.14 Schematic of Characteristics Measurement of the Antenna and Rectifier Circuit	43
Figure 4.15 Picture of Light-Weight Flexible Patch Antenna and Rectenna	44
Figure 4.16 Schematic of Antenna	45
Figure 4.17 Picture of Powere Sensor (HP 437B)	46
Figure 4.18 Picture of Power Meter (HP 8481A)	46
Figure 4.19 Picture of Adjustable Resistor	47
Figure 4.20 Schematics of Circuit of Measurement of the Loded Output Voltage	47
Figure 4.21 Picture of Digital Multi Meter (kaise KU-1188)	48
Figure 4.22 Picture of Signal Generator (Hittite HMC-T2000)	48
Figure 4.23 Picture of Network Analyzer (HP 8722D)	49
Figure 4.24 Picture of Mounting Structure	50
Figure 4.25 Picture of Electrical Motor	51
Figure 4.26 Picture of MAV model	52
Figure 4.27 Picture of the Rectennas on the MAV model	53
Figure 4.28 Picture of the MAV Demonstration Setup	53
Figure 5.1 Picture of Liner-Polarized Wave Antenna	54
Figure 5.2 Picture of Circular-Polarized Wave Antenna and Antenna Size	55
Figure 5.3 Polarized Wave Properties	56
Figure 5.4 Return Loss of the Light-Weight Flexibel Antenna	57
Figure 5.5 Picture of Antenna and Bend Definition	58
Figure 5.6 Bending Properties of the Light-Weigh Flexible Antenna	58
Figure 5.7 Schematic of Rectifier Circuit Pattern Parameters	60
Figure 5.8 Load Characteristic related to Capacitance of Chip Condenser	61

Figure 5.9 Load Characteristic related to D-G length	62
Figure 5.10 Schematic of Rectifier Circuit Pattern	63
Figure 5.11 Load Characteristic related to Number of LPFs	63
Figure 5.12 Load Characteristic related to Input Line Width	64
Figure 5.13 Load Characteristic related to Diode	65
Figure 5.14 Load Characteristic of New and Pre desig	66
Figure 5.15 Pictures of the Circuit and Bending definition	67
Figure 5.16 Bending Properties of the Light-Weigh Flexible RF-DC Conversion Circuit	67
Figure 5.17 Conversion Efficiency related to Input Power	68
Figure 5.18 Schematic of Rectenna Array Pitch	69
Figure 5.19 Picture of Rectenna with two antennas and one rectifier	70
Figure 5.20 Schematic of Parallel Connection of Rectenna	72
Figure 5.21 Schematic of Total Efficiency in Receiving System	73
Figure 5.22 DC Power related to Angle	74

List of tables

Table 1.1 Classifications of EMR	3
Table 4.1 Specifications of Transmitting Array Antenna System	34
Table 4.2 Specifications of Oscillator	35
Table 4.3 Specification of the Driver Amplifier	38
Table 4.4 Specification of Booster Amplifier	40
Table 4.5 Specification of the Antenna	45
Table 4.6 Specification of the Motor	51
Table 4.7 Specification of MAV model	52
Table 5.1 Return Loss and Resonance Frequency of Antennas	55
Table 5.2 Specifications of Circular-Polarized Wave Antenna	55
Table 5.3 Bending Properties and Efficiency of the Light-Weight Flexible Antenna	58
Table 5.4 Parameters for Standard Rectifier Circuit Pattern	60
Table 5.5 Specifications of four Diodes	65
Table 5.6 Parameters of New Design Rectifier Circuit Pattern	66
Table 5.7 Measurement Result of each array pitch	69
Table 5.8 Output Voltage of each rectenna	70
Table 5.9 Comparison with some rectennas	71

Chapter 1

Introduction

This chapter shows the background and the purpose of this thesis.

1.1 Wireless Power Transmission

Power supply methods are generally wire transmission methods using power line from power stations and codes from consents. However information-communication technology is become to be wireless, for examples television, radio, mobile phone and wireless LAN. Therefore power supply system changes from wire to wireless. Today, a lot of research and development about mobile ubiquitous equipments and wireless power supply are conducted for short charging time, easier charging, home appliance which can be anywhere, light battery capacity or resources and environment preservation such as reduction of code and harness which are around room and car.^{[1],[2]} Wireless Power Transmission is divided into some parts for the transmission range as in Figure 1.1.

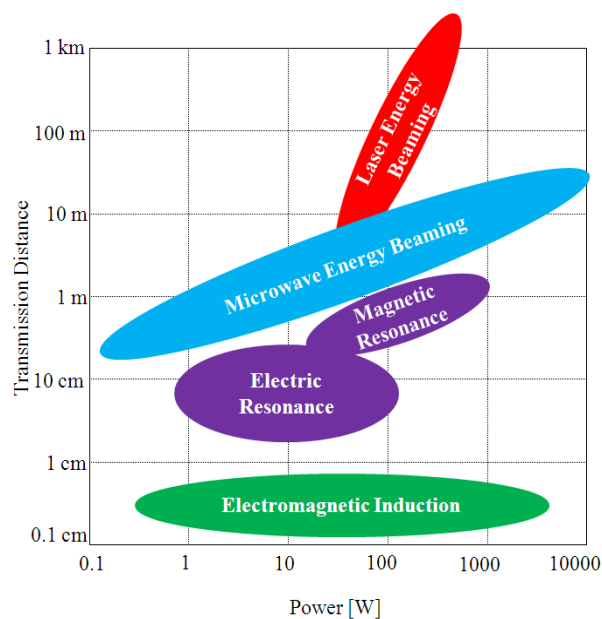


Figure 1.1 Classification of Wireless Power Transmission

Power supplying in short range is generally used electromagnetic induction. Electromagnetic induction is the production of voltage across a conductor moving through a magnetic field. This electromagnetic induction method of wireless power transmission has small power loss but short transmission range. The applications are, for example, passenger's cards of trains and buses and electric money cards.

Secondly, wireless power transmission in middle range is explained. Middle range means about $L/D = 1$ length, which D is antenna's size and L is transmission length. In the range, we are not able to transmit power effectively using electromagnetic induction method. Instead of the electromagnetic induction method, in the range, we can use strongly-coupled resonance method. The method is new technique and Professor Marin Soljacic et al. at MIT^[3] reported in 2006. In the theory, used not electromagnetic wave but electric or magnetic field, the power is transmitted from dielectric or resonating valance bond to the receiver. Because of this advantage such as longer transmission range and higher efficiency than the induction method, the strongly-coupled resonance method receives much attention as a new technique of wireless power transmission.

Finally, there is electromagnetic beam radiation method as technology of wireless power transmission to further range than wavelength. It is generally thought that electromagnetic radiation cannot transmit power sufficiently because the radiation diffuses with the transmission length. However a formation of electromagnetic beam makes the transmission length be extremely longer with small loss. This technology have been mainly focused on the space field, so power transmission to lunar probe using laser^[4] and large power transmission from solar power satellite to the ground^[5] have studied. Recently there has been interest in wireless power supply of robots and unmanned aircrafts.

1.2 Microwave Wireless Power Transmission

Electromagnetic radiation (EMR) is a form of energy exhibiting wave like behavior as it travels through space. EMR has both electric and magnetic field components, which oscillate in phase perpendicular to each other and perpendicular to the direction of energy propagation. EMR is applied to lots of technologies such as information-communication technology. Table 1.1 shows classifications of frequency of EMR and these applications.

Table 1.1 Classifications of EMR

Wave length	Frequency [Hz]	Name	Applications
10 ~ 1km	30k ~ 300k	Long Frequency (LF)	Aeronautical radio Marine radio
1km ~ 100m	300k ~ 3M	Middle Frequency (MF)	AM radio
100 ~ 10m	3M ~ 30M	High Frequency (HF)	Shortwave broadcast
10m ~ 1m	30M ~ 300M	Very High Frequency (VHF)	FM radio
1m ~ 10cm	300M ~ 3G	Ultra High Frequency (UHF)	Mobile phone Microwave oven
10cm ~ 1cm	3G ~ 30G	Super High Frequency (SHF) Microwave	Satellite broadcasting
1cm ~ 1mm	30G ~ 300G	Extremely High Frequency (EHF) Millimeter wave	Satellite communications
1mm ~ 0.1mm	300G ~ 3T	Submillimeter wave	

Microwaves are electromagnetic waves with wavelength ranging from as long as one meter to as short as one millimeters, or equivalently, with frequencies between 0.3 GHz and 300 GHz. In all cases, microwave includes the entire SHF band (3 to 30 GHz, or 10 to 1 cm) at minimum, with RF engineering often putting the lower boundary at 1 GHz (30 cm), and the upper around 100 GHz (3 mm). Microwave technology is first developed as radar technology in 1940s. The radar uses the characteristics of microwaves which travel in a straight line because of the short wavelength and reflect off an object which has size above the wavelength. After that microwaves have had a wide filed of application because of the advantage of straight traveling and the large transmission capacity of information. Microwaves are applied to mobile phones and satellite communications as transmission signals, microwave ovens using dielectric heat of microwaves, radio astronomy, particle acceleration and medical devices. Then microwave technology has attracted much attention.

Microwave Wireless Power Transmission (MWPT) is first reported by W. C. Brown in 1960s^[6].^[7] Since he succeeded microwave power transmission to a helicopter (Figure 1.2), MWPT is applied to large applications such as Solar Power System in space (SPS) and also small applications such as micro robots which can move with small power because MWPT has long transmission range.



Figure 1.2 Experiment of MWPT to a helicopter

1.3 MWPT to Micro Aerial Vehicle and Purpose of the thesis

Conventional transportation systems, for example cars and aircrafts, are able to have long running distances and high mobility with loading some fuels of high energy densities. However it is difficult to replace such abilities to battery's abilities. To run longer without power supply, the systems need larger capacities of charge. Therefore batteries need more mineral resources, the weight of the batteries is larger than that of passengers and loads and the total efficiency become to be lower. To decrease the weigh and load of the batteries, the systems need to be supplied power frequently at the supply station, so techniques of wireless power transmission are necessary. Micro robots, which developed for surveillance and checking of devastated district, medical examination of body and so on, are used. However the robots sometimes cannot move with their size, wire and weight. Without batteries, their duration, size and range of moving are not be regulated. These days ICs, sensors and LEDs have been developed at mW levels, so higher functions devices without batteries are able to be designed and new applications are expected.

Micro Aerial Vehicle (MAV) is a power beaming system and an unmanned aircraft^{[8] - [15]}. With this wireless power transmission system, a battery on a vehicle is charged by receiving a microwave beam while the vehicle is circling above a phased array transmitter. Then, it can fly over the area struck by disaster, for example, continuously without landing and take-off for recharging. Figure 1.3 shows the schematic of the system developed in our laboratory. It consists of three sub-systems; a transmission system^{[8], [10], [11], [14], [15]}, a tracking system^{[8], [10], [11], [14], [15]}, and a receiving system^{[9], [12], [13]}. The MAV is tracked using the phase information of pilot signal. Software retro-directive function has been realized through a PC control and a microwave beam is pointed to the MAV using an active phased array. An electric motor for a propeller is driven by the power received on a rectenna array. Rectenna has antenna and RC-DC conversion circuit which converts microwave power to DC power.

Generally, conventional rectennas are made by etching copper foils based on solid dielectric boards. However the geometry of a MAV is often curvature, therefore rectenna should be flexible to utilize the geometry at a maximum. In addition the MAV should be light weight, so rectenna is also necessary to be light weight. However, few studies have been reported on the light weight and flexible rectennas, and very few other studies of the high efficiency, light weight and flexible patch rectennas has appeared.

The purpose of this study has been to develop a light-weight flexible patch rectenna for the MAV system and to demonstrate the MAV system especially the receiving system.

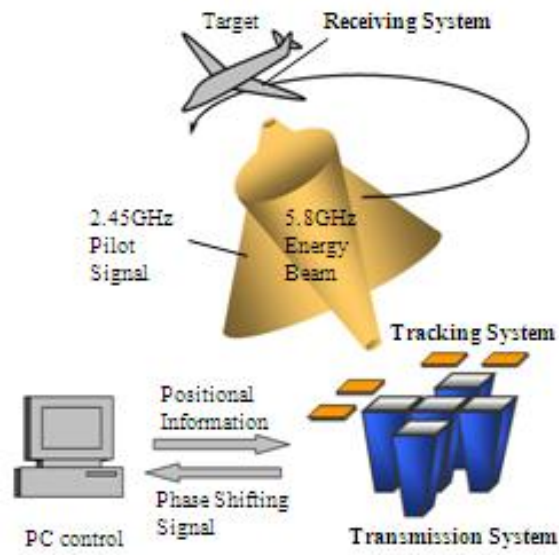


Figure 1.3 Schematic of the MAV system

Chapter 2

Basic Theory

This chapter is explained about microwave basic theory. Further details or information are written in “Microwave Engineering^[16]”.

2.1 Wave Propagation and Polarization

There are two polarized waves; linear polarized wave and circular polarized wave. I explain the polarization theories and the reasons why the polarity-free antennas are needed below.

2.1.1 Linear polarized wave

Electromagnetic wave, including microwave, has a polarization. When an electromagnetic wave propagates through an uniform medium, the Maxwell equations are expressed with a charge density $\rho=0$ as:

$$\left. \begin{aligned} \nabla \times \mathbf{E} &= -\mu \frac{\partial \mathbf{H}}{\partial t} \\ \nabla \times \mathbf{H} &= \sigma \mathbf{E} + \varepsilon \frac{\partial \mathbf{E}}{\partial t} \\ \nabla \cdot \mathbf{E} &= 0 \\ \nabla \cdot \mathbf{H} &= 0 \end{aligned} \right\} \quad (2.1)$$

where ε is a dielectric constant and μ is a conductivity of the medium. Generally, an electromagnetic wave varies at a constant frequency as sine curve, the electric field \mathbf{E} and the magnetic field \mathbf{H} are expressed as:

$$\mathbf{E} = \mathbf{E}_0 e^{i\omega t} \quad (2.2)$$

$$\mathbf{H} = \mathbf{H}_0 e^{i\omega t} \quad (2.3)$$

where ω is an angular frequency. Since they include phase terms, these \mathbf{E} , \mathbf{E}_0 , \mathbf{H} , \mathbf{H}_0 are complex variables and the absolute values of \mathbf{E}_0 , \mathbf{H}_0 are the amplitude of the electric field and that of the magnetic field. The real waves are expressed by their real parts.

Moreover, let the partial differentiation about time t $\partial/\partial t = j\omega$ and divide the electrical field

and the magnetic field to x , y and z element, then the equation (2.1) is converted as:

$$\left. \begin{aligned} \frac{\partial E_z}{\partial y} - \frac{\partial E_y}{\partial z} &= -j\omega\mu H_x \\ \frac{\partial E_x}{\partial z} - \frac{\partial E_z}{\partial x} &= -j\omega\mu H_y \\ \frac{\partial E_y}{\partial x} - \frac{\partial E_x}{\partial y} &= -j\omega\mu H_z \\ \frac{\partial H_z}{\partial y} - \frac{\partial H_y}{\partial z} &= (\sigma + j\omega\varepsilon)E_x \\ \frac{\partial H_x}{\partial z} - \frac{\partial H_z}{\partial x} &= (\sigma + j\omega\varepsilon)E_y \\ \frac{\partial H_y}{\partial x} - \frac{\partial H_x}{\partial y} &= (\sigma + j\omega\varepsilon)E_z \end{aligned} \right\} \quad (2.4)$$

When an electromagnetic wave propagates as a planar wave, there is no change of the electric field and the magnetic field in the x - y plane at right angles to the propagating direction (z axis). Or the solutions differentiating these fields with respect to x and y are 0. Under this condition, the z axial component of the electromagnetic field varying temporally is expressed as:

$$E_z = H_z = 0 \quad (2.5)$$

Figure 2.1 shows the electromagnetic wave called “transverse electro magnetic (TEM) wave” or “linear polarized wave;” the temporally homogeneous electromagnetic wave without the component in the propagation direction of the electric field and the magnetic field. Additionally the plane formed by the direction of the electric field and the wave propagating direction is called the “polarization plane.”

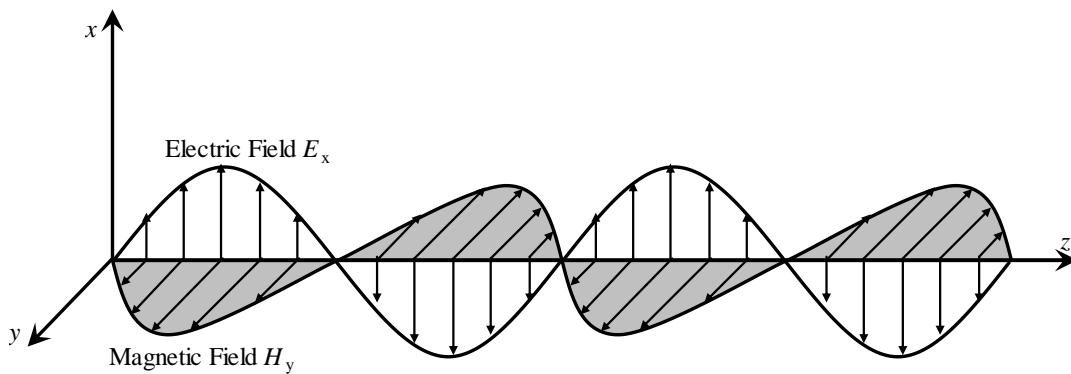


Figure 2.1 Schematic of Planar wave (TEM) Propagation

As a result, the equation (2.4) is figured as:

[x-direction polarization]

$$\begin{aligned}\frac{\partial E_x}{\partial z} &= -j\omega\mu H_y \\ \frac{\partial H_y}{\partial z} &= -(\sigma + j\omega\varepsilon)E_x\end{aligned}\quad (2.6)$$

[y-direction polarization]

$$\begin{aligned}\frac{\partial E_y}{\partial z} &= -j\omega\mu H_x \\ \frac{\partial H_x}{\partial z} &= -(\sigma + j\omega\varepsilon)E_y\end{aligned}\quad (2.7)$$

The x -direction polarization has only an x component of the electric field and a y component of the magnetic field as Figure 2.1, and the y -direction polarization is the equivalent of the x -direction one rotated by 90 degrees around the propagation direction. Furthermore, they can exist independently of each other. With the linear polarized wave, we can obtain power only with the antennas of the same polarization as the incident wave: the set of horizontal antennas and horizontal wave, or of vertical antennas and vertical wave.

2.1.2 Circular polarized wave

Linear polarized waves are able to generate only artificially, and the polarization plane of natural electromagnetic waves are temporally rotating. Figure 2.2 shows its schematic. It is called “circular polarized wave.” We can generate circular polarized waves by combining the linear polarized waves.

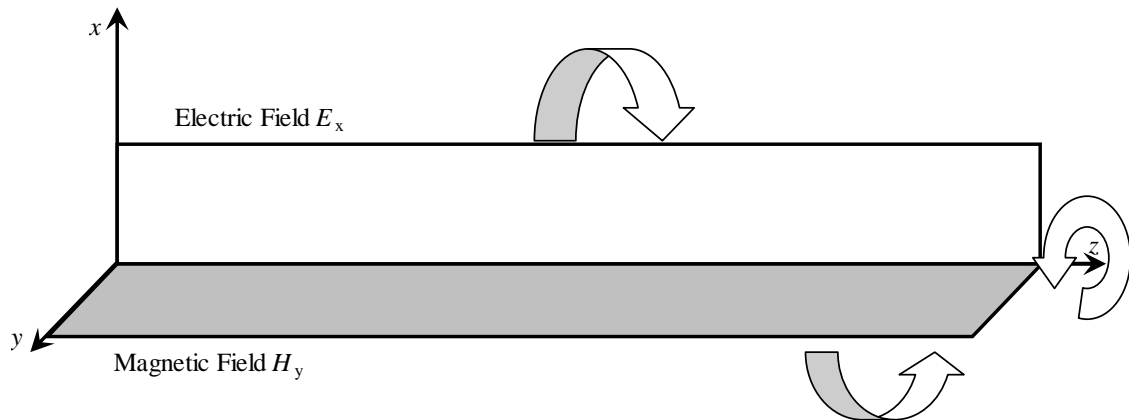


Figure 2.2 Schematic of Rotating Polarization Plane

When there are two linear polarized waves, the electric field component of the x -direction polarized wave is expressed as:

$$E_x = a \cos(\omega t - \beta z) \quad (2.8)$$

where β is a phase constant, and that of the y -direction polarized wave with the phase delaying by δ is also expressed as:

$$E_y = b \cos(\omega t - \beta z - \delta) \quad (2.9)$$

When two polarized waves with different phases exist, the circular polarized wave is generated with combining them. (When there is no phase difference, or $\delta=0$, the combined wave is just a linear polarized wave at an angle with the x -axis.)

Under the special condition where $\delta=\pi/2$, $a=b$, E_x and E_y are represented as:

$$\left. \begin{aligned} E_x &= a \cos(\omega t - \beta z) \\ E_y &= a \cos(\omega t - \beta z - \pi/2) = a \sin(\omega t - \beta z) \end{aligned} \right\} \quad (2.10)$$

and then:

$$E_x^2 + E_y^2 = a^2 \quad (2.11)$$

From this, the combined electric field plane is rotating around any z position within its radius a . In turn, this wave is propagating to the z direction at the phase velocity v_p with rotating around the z -axis at the angular rate ω . This wave called ‘‘circular polarized wave.’’ Under the general condition where not both $\delta=\pi/2$ and $a=b$, the field locus is the ellipse and the wave called ‘‘elliptical polarized wave.’’

2.1.3 Polarization Choice for MAV

In this thesis, since the objective was the power transmission, not signal transmission, I needed the high-efficient and simple system. The circular polarized wave can ignore the characteristic of the polarization plane. However, it is unsuitable for the power transmission because of its lower transmitting efficiency by reflections with transmitting and receiving than the linear one. The linear one can achieve high efficiency and simple control system, then as with many researches, I adopted it for the power transmitting system. Furthermore, since the MAV will move with random yaw angle in spite of the fixed polarization plane by the linear polarized transmitting wave, we need to make the receiving device polarity-free.

2.2 Transmission Line Theory

In many ways transmission line theory bridges the gap between field analysis and basic circuit theory, and so is of significant importance in microwave analysis.

2.2.1 Wave Propagation on a Transmission Line

As shown in Figure 2.3a, a transmission line is often schematically represented as a two-wire line, since transmission lines always have at least two conductors. The short piece of line of length Δz of Figure 2.3a can be modeled as a lumped-element circuit, as shown in Figure 2.3b, where R , L , G , C are per unit length quantities defined as follows:

R = series resistance per unit length, for both conductors, in Ω/m .

L = series inductance per unit length, for both conductors, in H/m .

G = shunt conductance per unit length, in S/m .

C = shunt capacitance per unit length, in F/m .

From the circuit of Figure 2.3b, Kirchhoff's voltage and current law can be applied to give

$$v(z, t) - R\Delta z i(z, t) - L\Delta z \frac{\partial i(z, t)}{\partial t} - v(z + \Delta z, t) = 0, \quad (2.12)$$

$$i(z, t) - G\Delta z v(z + \Delta z, t) - C\Delta z \frac{\partial v(z + \Delta z, t)}{\partial t} - i(z + \Delta z, t) = 0. \quad (2.13)$$

Dividing (2.12) and (2.13) by Δz and taking the limit as $\Delta z \rightarrow 0$ gives the following differential equations:

$$\frac{\partial v(z, t)}{\partial z} = -Ri(z, t) - L \frac{\partial i(z, t)}{\partial t}, \quad (2.14)$$

$$\frac{\partial i(z, t)}{\partial z} = -Gv(z, t) - C \frac{\partial v(z, t)}{\partial t}. \quad (2.15)$$

These equations are the time-domain form of the transmission line, or telegrapher, equations.

For the sinusoidal steady-state condition, with cosine-based phasors, (2.14) and (2.15) simplify to

$$\frac{dV(z)}{dz} = -(R + j\omega L)I(z), \quad (2.16)$$

$$\frac{dI(z)}{dz} = -(G + j\omega C)V(z). \quad (2.17)$$

The two equations of (2.16) and (2.17) can be solved simultaneously to give wave equations for $V(z)$ and $I(z)$:

$$\frac{d^2V(z)}{dz^2} - \gamma^2 V(z) = 0, \quad (2.18)$$

$$\frac{d^2I(z)}{dz^2} - \gamma^2 I(z) = 0, \quad (2.19)$$

where
$$\gamma = \alpha + j\beta = \sqrt{(R + j\omega L)(G + j\omega C)} \quad (2.20)$$

is the complex propagation constant, which is a function of frequency. Traveling wave solutions to (2.18) and (2.19) can be found as

$$V(z) = V_o^+ e^{-\gamma z} + V_o^- e^{\gamma z}, \quad (2.21)$$

$$I(z) = I_o^+ e^{-\gamma z} + I_o^- e^{\gamma z}. \quad (2.22)$$

where the $e^{-\gamma z}$ term represents wave propagation in the $+z$ direction, and the $e^{\gamma z}$ term represents wave propagation in the $-z$ direction.

Comparison with (2.21) and (2.22) shows that a characteristic impedance, Z_0 , can be defined as

$$Z_0 = \frac{R + j\omega L}{\gamma} = \sqrt{\frac{R + j\omega L}{G + j\omega C}}, \quad (2.23)$$

Then (2.22) can be rewritten in the following form:

$$I(z) = \frac{V_o^+}{Z_0} e^{-\gamma z} - \frac{V_o^-}{Z_0} e^{\gamma z}. \quad (2.24)$$

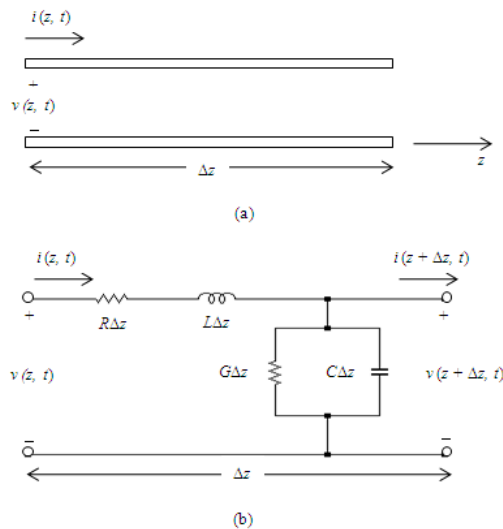


Figure 2.3 Voltage and current definitions and equivalent circuit

2.2.2 The Lossless Line

The above solution was for a general transmission line, including loss effects, and it was seen that the propagation constant and characteristic impedance were complex. In many practical cases, however, the loss of the line is very small and so can be neglected, resulting in a simplification of the above results. Setting $R = G = 0$ in (2.20) gives the propagation constant as

$$\gamma = \alpha + j\beta = j\omega\sqrt{LC}, \quad (2.25)$$

or
$$\beta = \omega\sqrt{LC}, \quad (2.26)$$

$$\alpha = 0, \quad (2.27)$$

where γ is the propagation constant, β is the phase constant and α is the attenuation constant. As expected for the lossless case, the attenuation constant α is zero. The characteristic impedance of (2.23) reduces to

$$Z_0 = \sqrt{\frac{L}{C}}, \quad (2.28)$$

which is now a real number. The general solutions for voltage and current on a lossless transmission line can then be written as

$$V(z) = V_o^+ e^{-j\beta z} + V_o^- e^{j\beta z}, \quad (2.29)$$

$$I(z) = \frac{V_o^+}{Z_0} e^{-j\beta z} - \frac{V_o^-}{Z_0} e^{j\beta z}. \quad (2.30)$$

The wavelength is

$$\lambda = \frac{2\pi}{\beta} = \frac{2\pi}{\omega\sqrt{LC}}, \quad (2.31)$$

and the phase velocity is

$$v_p = \frac{\omega}{\beta} = \frac{1}{\sqrt{LC}}. \quad (2.32)$$

2.2.3 The Terminated Lossless Transmission Line

Figure 2.4 shows a lossless transmission line terminated in an arbitrary load impedance Z_L . Assume that an incident wave of the form $V_o^+ e^{-j\beta z}$ is generated from a source at $z < 0$. The total voltage and total current on the line can be written as in (2.29) and (2.30), as a sum of incident and reflected waves. The total voltage and current at the load are related by the load impedance, so at $z = 0$ we must have

$$Z_0 = \frac{V(0)}{I(0)} = \frac{V_o^+ + V_o^-}{V_o^+ - V_o^-} Z_0. \quad (2.33)$$

The amplitude of the reflected voltage wave normalized to the amplitude of the incident voltage wave is known as the voltage reflection coefficient, Γ :

$$\Gamma = \frac{V_o^-}{V_o^+} = \frac{Z_L - Z_0}{Z_L + Z_0}. \quad (2.34)$$

When the load is mismatched, then, not all of the available power from the generator is delivered to the load. This “loss” is called *return loss* (RL), and is defined (in dB) as

$$\text{RL} = -20 \log |\Gamma| \text{ dB}. \quad (2.35)$$

At a distance $l = -z$ from the load, the input impedance seen looking toward the load is

$$Z_{in} = \frac{V(-l)}{I(-l)} = \frac{V_o^+ \left[e^{j\beta l} + \Gamma e^{-j\beta l} \right]}{V_o^+ \left[e^{j\beta l} - \Gamma e^{-j\beta l} \right]} Z_0 = \frac{1 + \Gamma e^{-2j\beta l}}{1 - \Gamma e^{-2j\beta l}} Z_0, \quad (2.36)$$

by using (2.34) for Γ in (2.36):

$$Z_{in} = Z_0 \frac{Z_L + jZ_0 \tan \beta l}{Z_0 + jZ_L \tan \beta l}. \quad (2.37)$$

This is an important result giving the input impedance of a length of transmission line with an arbitrary load impedance.

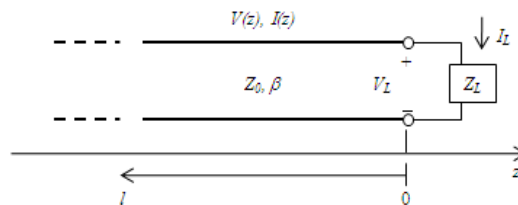


Figure 2.4 A transmission line terminated in a load impedance Z_L

Chapter 3

Theories of Rectenna elements

This chapter shows the theories of the rectenna elements including antenna elements and rectifier circuit elements. Further details and information are written in “Antenna Theory and Design Revised Edition^[17]”.

3.1 Theory of Rectenna Design

“Rectenna” is a device receiving the transmitted microwave power as radio frequency (RF) and converting alternating current (AC) to direct current (DC) by rectifying. It is the coined term for “RECTifier” and “antENNA”. Figure 3.1a shows its schematic. It normally consists of a receiving antenna, an input filter, a rectifier and a output filter for smoothing power. Since the receivable power with a rectenna is not enough large to operate systems, we use as a array of some rectennas arranged and connected in series and in parallel each other.

One of the determining factors of the power conversion efficiency of a rectenna is the characteristic of the important element of a rectifier, or a diode^[18]. Figure 3.1b shows the RF-DC conversion efficiency characteristic of a rectenna. When the input power P_{in} decrease, the conversion efficiency η will become reduced. It is because the voltage between the both ends of a diode V_d will become smaller than the diode forwarding voltage V_f , and then the rectifying feature of the diode will not work (the V_f effect). Although the conversion efficiency increase as P_{in} becomes larger, when V_d surpass the diode breakdown voltage V_R , η will also become reduced. It is because the reverse current starts to flow (the V_R effect). Moreover, η will also become reduced because the high order radio-frequency re-radiation generated with rectifying (the higher order harmonics effect).

Furthermore, the load resistance connected to the rectenna output has the optimal values; it is the value in matching the output impedances of the rectenna with the load and also depends on P_{in} . Although there is no reflected wave with connecting the optimal load, there is reflected waves and η decreased without it. As a result, the diode maximum efficiency curve has a peak value depending on the input power P_{in} and the load resistance R_L .

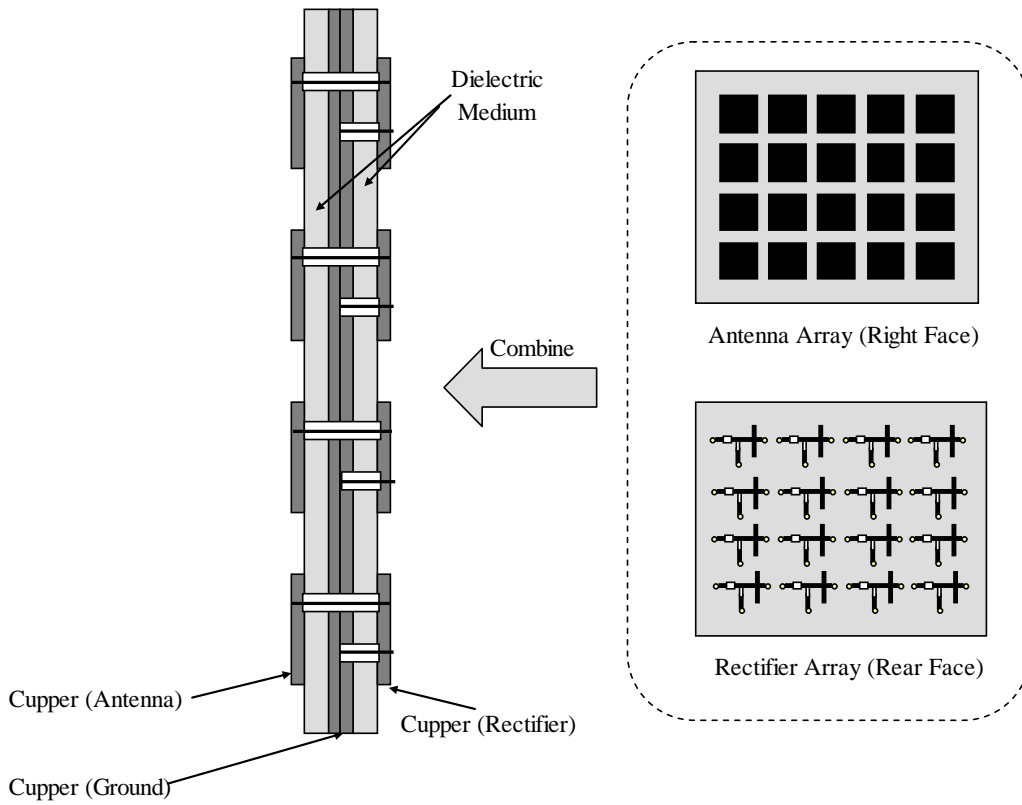


Figure 3.1a Schematic of Rectenna

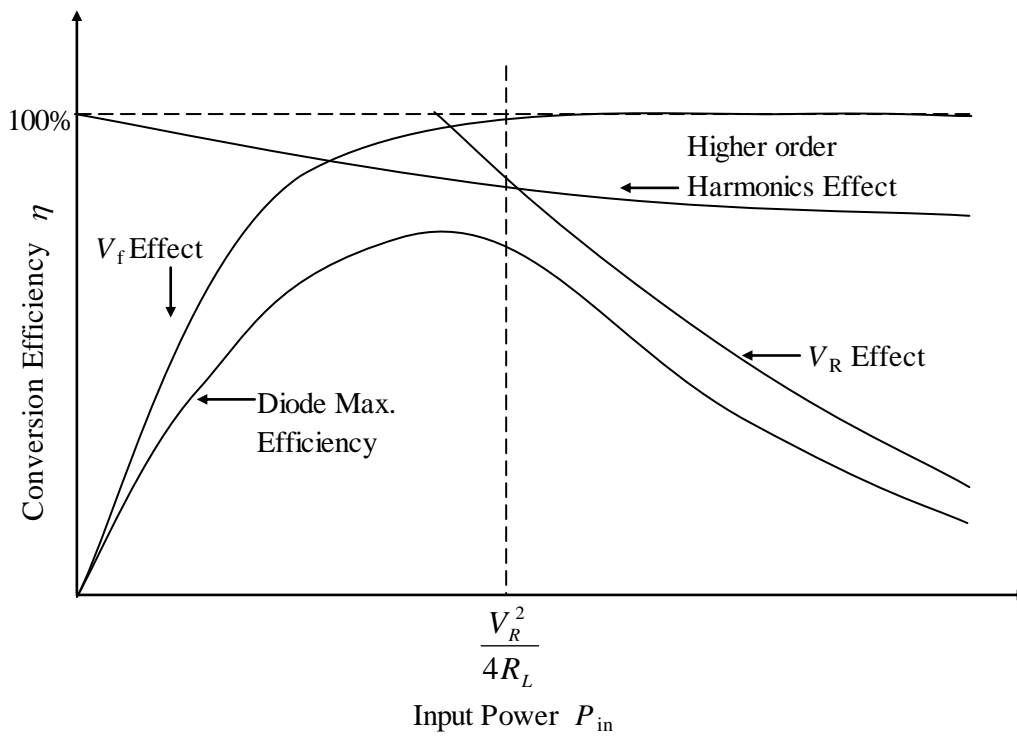


Figure 3.1b RF-DC Conversion Efficiency of Rectenna

3.2 Theory of Antenna Design

There are many kinds of Antenna; horn antennas, monopole antenna, dipole antennas, slot antennas, *etc*^{[17], [19], [20]}. In this thesis, we adopted the plane patch antennas because of the simplicity of structure, the miniaturization in the size and the lightness.

The typical examples of the plane antennas are MSA (Micro Strip Antenna) elements. They function as the microwave radiators composed of the planar circuit resonance elements with the circular or quadrangular open boundary on the printed circuit boards (PCBs). Generally the substrate for the MSA require low dielectric constant ($\epsilon_r = 1.2 \sim 5.0$) and low dielectric loss ($\tan \delta = 10^{-3} \sim 10^{-4}$), such as the teflon-fiberglass substrate. In request for weight saving of wider band width (low Q value), the paper-honeycomb substrate are used.

The size of the MSA elements is normally the half wavelength or less. The main mode is used as a specimen excitation mode, and the MSA radiation pattern of the main mode shows the unidirectionality with the maximum value in the front direction (z -axis) of the antenna pattern of both the circular and quadrangular MSA. Thus, MSA enables to achieve the unidirectional pattern without additional reflectors and to compose the thin and compact antenna simply.

3.2.1 Size Designing of MSA

The size of antennas depends on the target microwave wavelength. Generally the half wavelength resonance method is used, and its resonance direction length is $\lambda_g/2$. The λ_g is the wavelength of the microwave passing through a medium and is approximately expressed by:

$$\lambda_g = \frac{\lambda_0}{\sqrt{\epsilon_r}} \quad (3.1)$$

where λ_0 is the free-space wavelength and ϵ_r is the dielectric constant of the medium. In this thesis, the size of square MSA for 5.8GHz was about 1.22cm on a side, 1.484cm² with the glass-epoxy substrate FR-4 ($\epsilon_r=4.7$). I explain the more details in 0.

3.2.2 Impedance Matching Method between MSA element and Feeding System

Figure 3.2 shows the typical feeding methods of the MSA. The input impedance Z_{in} of the MSA excited in the main mode depends on the predetermined feeding point ρ_0 ^[21]. Z_{in} at the resonance point and around the near frequency domain vary from 0 (center) to several hundred ohms (open boundary) by ρ_0 . Thus, with feeding at the edge (open boundary) of the MSA elements, the resonance Z_{in} exhibits a high impedance characteristic about 300~500 Ω . Consequently, we need for it to match up with the feeding system about 50 Ω of the characteristic impedance. In the backside-coaxial feeding method, we can match up the impedances by offsetting the position ρ_0 of the feeding point F. Generally, the offset ratio is about 30%; (ρ_0/a)=0.3 in the circular MSA,

($\rho_0/(a/2)=0.3$) in the quadrangular MSA. In the coplanar feeding method, we can also match up the impedance of the antenna with one of the main feeding line F_m by the $\lambda_g/4$ impedance transformer T_f . In the electromagnetic coupling feeding method, it is adopted to set the insert length l_0 to the specimen excitation slot of the feeding strip line at about $\lambda_g/4$, and to control the values of the specimen excitation slot width w , its slot length l_s and the offset length ρ_0 . In this thesis, we adopted the backside-coaxial feeding method and 0.3 of ρ_0 because of the simplicity of its fabrication and the connectivity with the rectifier circuits.

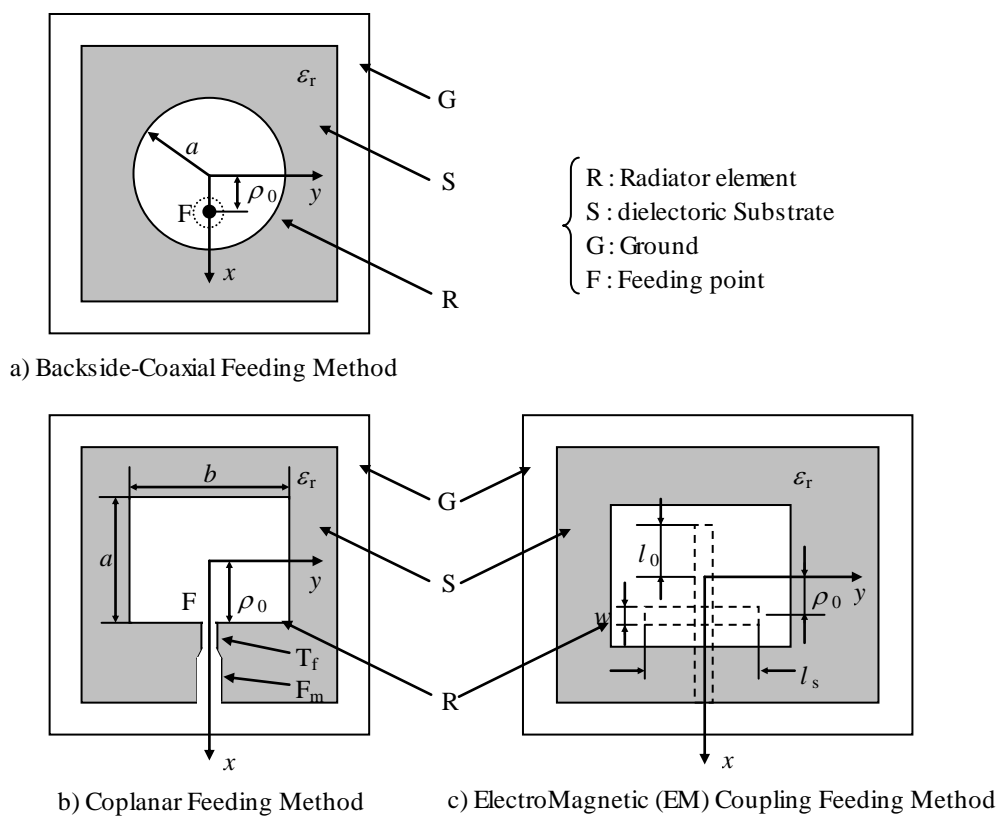
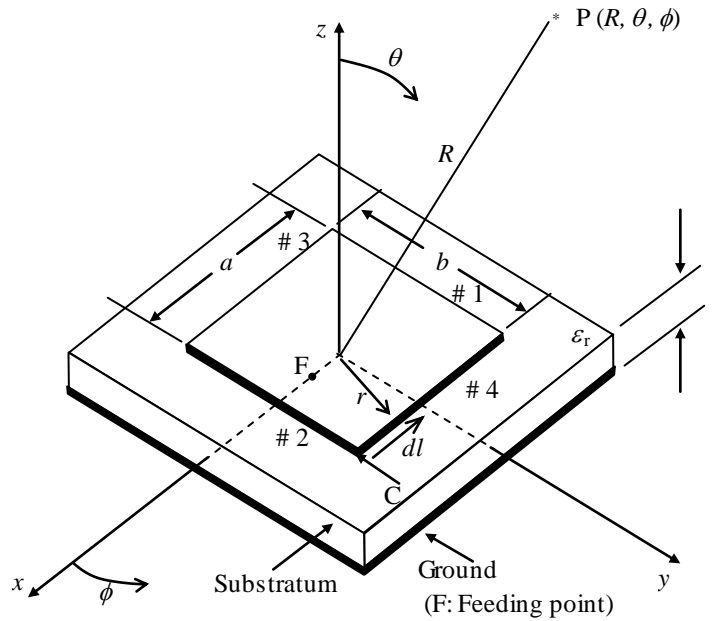


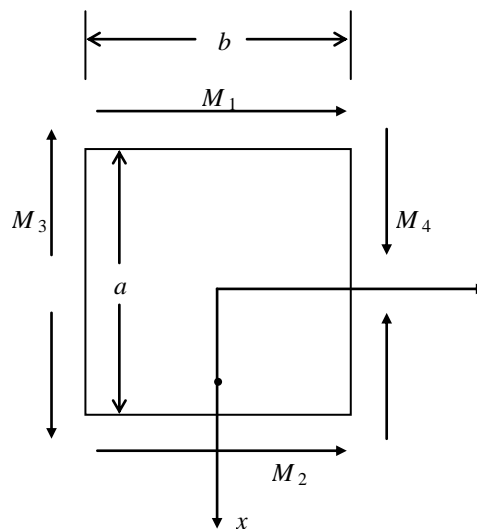
Figure 3.2 Feeding Methods of MSA Element

3.2.3 Interior Electromagnetic Field of Rectangular MSA

Figure 3.3 shows the analysis model of the inner electromagnetic field of a rectangular MSA. When the substrate thickness t is enough smaller than the free-space wavelength λ_0 ($k_0 t \ll 1$; k_0 is a free-space wavenumber), TM_{mn0} wave is excited; it has an electric field element only to the direction of t (z direction).



a) Coordinate System



b) Example of Magnetic Current

Figure 3.3 Rectangular MSA and its Coordinate System

The electromagnetic field of this TM_{m0} wave is expressed by follow wave equation:

$$\left(\nabla^2_t + k^2\right)E_z = 0 \quad (\text{Interior region}) \quad (3.2)$$

$$\frac{\partial E_z}{\partial n} = 0 \quad (\text{Open boundary}) \quad (3.3)$$

where \hat{n} is outward unit normal vector at the open boundary and ∇^2_t is $(\partial^2/\partial x^2 + \partial^2/\partial y^2)$.

When we separate variables of E_z element as $E_z=X(x)Y(y)$ and of k element as $k^2=k_x^2+k_y^2$ into x and y directions, and assign it to the equation (3.2):

$$\frac{1}{X} \frac{\partial^2 X}{\partial x^2} = -k_x^2 \quad (3.4)$$

$$\frac{1}{Y} \frac{\partial^2 Y}{\partial y^2} = -k_y^2 \quad (3.5)$$

where $k_x=m\pi/a$ of a wavenumber in x direction and $k_y=n\pi/b$ in y direction. by using the separation of variables, E_z element of TM_{m0} wave is expressed by:

$$E_z = E_0 \cos\left(\frac{m\pi}{a}x + \frac{m\pi}{2}\right) \cos\left(\frac{n\pi}{b}y + \frac{n\pi}{2}\right) \quad (3.6)$$

$$k^2 = (k_x^2 + k_y^2) = \left[\left(\frac{m\pi}{a}\right)^2 + \left(\frac{n\pi}{b}\right)^2 \right] \quad (3.7)$$

where E_0 is an arbitrary number, $k = \omega\sqrt{\varepsilon\mu}$ is the wavenumber in the dielectric, and m and n are arbitrary integers. Additionally, we assign this E_z to the Maxwell equation and consider the TM wave condition ($H_z=0$), then we can find the interior electromagnetic elements of the rectangular MSA as:

$$\left. \begin{aligned} E_z &= \frac{V_0}{t} \cos\left(\frac{m\pi}{a}x + \frac{m\pi}{2}\right) \cos\left(\frac{n\pi}{b}x + \frac{n\pi}{2}\right) \\ H_x &= -\frac{j\omega\varepsilon}{k^2} \cdot \frac{n\pi}{b} \cdot \frac{V_0}{t} \cos\left(\frac{m\pi}{a}x + \frac{m\pi}{2}\right) \sin\left(\frac{n\pi}{b}x + \frac{n\pi}{2}\right) \\ H_y &= \frac{j\omega\varepsilon}{k^2} \cdot \frac{m\pi}{a} \cdot \frac{V_0}{t} \cos\left(\frac{m\pi}{a}x + \frac{m\pi}{2}\right) \cos\left(\frac{n\pi}{b}x + \frac{n\pi}{2}\right) \\ E_x &= E_y = H_z = 0 \end{aligned} \right\} \quad (3.8)$$

where $V_0=tE_0$ is the peak voltage at the edge of the MSA element as a magnetic wall.

In the normal application of the rectangular MSA, TM_{100} or TM_{010} wave as the lowest order mode (basic mode) is important. The interior electromagnetic field of This TM_{100} wave can be find by the equation (3.8) as:

$$\left. \begin{aligned} E_z &= -\frac{V_0}{t} \sin\left(\frac{\pi}{a}x\right) \\ H_y &= \frac{j\omega\varepsilon}{k^2} \cdot \frac{\pi}{a} \cdot \frac{V_0}{t} \cos\left(\frac{\pi}{a}x\right) \\ E_x = E_y = H_x = H_z &= 0 \end{aligned} \right\} \quad (3.9)$$

and Figure 3.4 shows the schematic of its electromagnetic distribution considering the edge effect.

Furthermore we can find the resonance frequency f_r of TM_{100} wave with assigning $m=1$, $n=0$ and $k = \omega\sqrt{\varepsilon\mu}$ as:

$$f_r = \frac{v_0}{2a\sqrt{\varepsilon_r}} \quad (3.10)$$

where v_0 is the light speed, ε_r is the dielectric constant of the specimen substratum. When we calculate the resonance frequency of the rectangular MSA, we need to consider the fringing effect:

$$f_r = \frac{v_0}{2a_{\text{eff}}\sqrt{\varepsilon_r}} \quad (3.11)$$

where a_{eff} is the equivalent side length and ε_e is the effective dielectric constant, and they are expressed as:

$$\left. \begin{aligned} a_{\text{reff}} &= a \left\{ 1 + 0.824 \frac{t}{a} \cdot \frac{(\varepsilon_e + 0.3)[(a/t) + 0.262]}{(\varepsilon_e - 0.258)[(a/t) + 0.813]} \right\} \\ \varepsilon_e &= \frac{\varepsilon_r + 1}{2} + \frac{\varepsilon_r - 1}{2} \left(1 + 10 \frac{t}{a} \right)^{-0.5} \end{aligned} \right\} \quad (3.12)$$

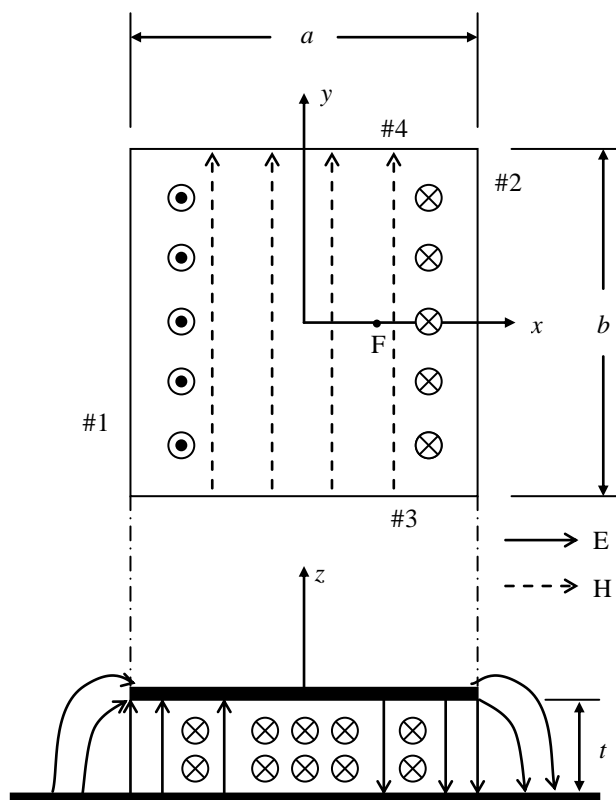


Figure 3.4 Schematic of Electromagnetic Distribution of TM_{100} wave

3.2.4 Methods for Polarity-free Antenna

Generally, there are two methods to make receiving antennas polarity-free: one method is a unit of multiple antennas (UMA) with different polarization angles, and another is a self polarity-free antenna (SPFA).

The UMA method is making an antenna-unit combining some normal polarized antennas, such as dipole antennas and patch antennas, and arranging them in predetermined design. It enables to supply stable power as the unit by antenna elements covering for each other's weak angles. Figure 3.5 shows the unit of multiple dipole antennas (UMDA). One of the advantages is the calculation simplicity of the polarization-angle dependency and the power conversion efficiency because the UMA consists of the existing antennas. Furthermore, a flexible UMDA sheet has been developed. However, the disadvantages are the low conversion efficiency and the large size because it needs some antennas for achieving polarity-free and the utilizable power is the average obtained from them. Moreover, some rectifier circuits are also needed.

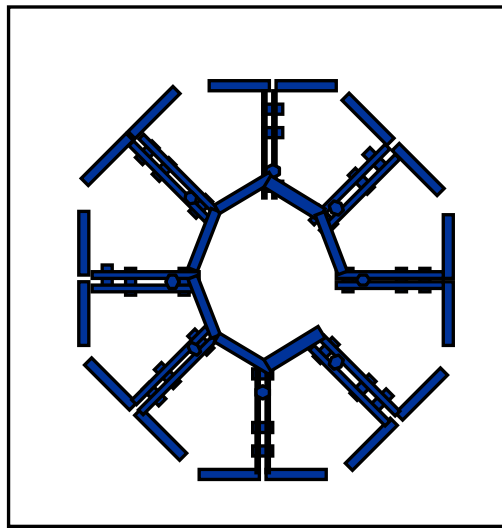


Figure 3.5 Pattern of Unit of Multiple Dipole Antenna

The SPFA method is making an antenna itself polarity-free without any excessive antenna area. The advantage is the smallness of its minimum unit area; about one ninth the size of the UMDA. Moreover, since it requires only one rectifier circuit in a unit, its structure is very simple. These advantages are suitable for the MAV-installed system. However, the disadvantage is the design; the completely SPFA has not been reported. Therefore, I surveyed the SPFA design based on patch antenna for circular polarized wave (ACPW) in Figure 3.6.

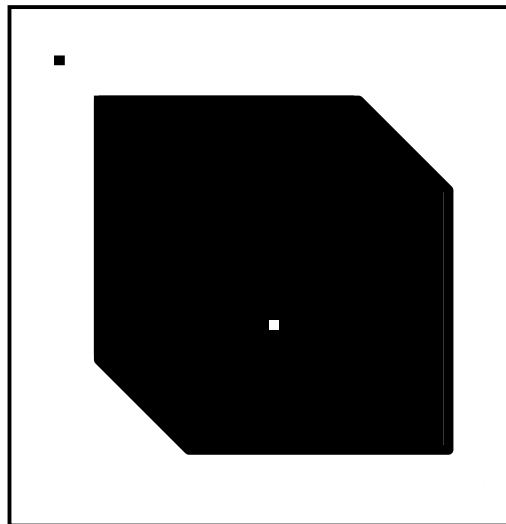


Figure 3.6 Pattern of Patch Antenna for Circular Polarized Wave

3.3 Theory of Rectifier Circuit Design

In order to develop the power conversion efficiency of a rectifier, we need its accurate output equivalent circuit model^{[22], [23]}. There are two independent approaches. Firstly, an approximate closed-form circuit was developed assuming an ideal diode and lossless circuit elements. The output equivalent circuit was obtained analytically. Secondly, a more precise computer-simulation model was used, and the load resistance and plotting the resultant output load line. In other researches, numerous rectifier circuits are possible, and a single shunt model diode rectifier circuit has proven most useful in the development work. Figure 3.7 shows an idealized equivalent circuit of this rectifier. The input filter should prevent any of the direct current (DC) and harmonic to flow back through the antenna resistance R_S , but allow current flow at the fundamental radio frequency (RF) ω . The output filter should not only prevent alternating current (AC) components to appear across the load terminals but also allow harmonic currents to flow. In particular, the even harmonics should be allowed to flow since they have the property of having a zero average on each half cycle (harmonics are in phase with respect to fundamental). Therefore, the output filter should allow the even harmonics to flow without any voltage drop, prevent current flow at any of the odd harmonics, and allow DC current flow.

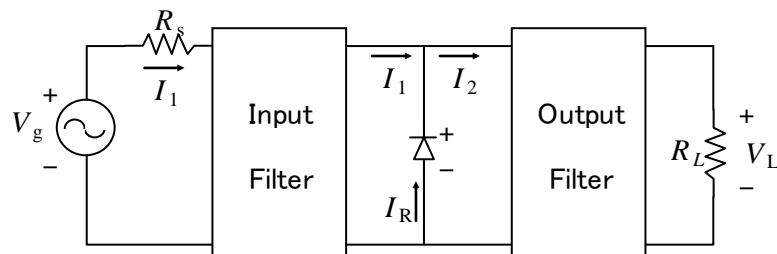


Figure 3.7 Simple Schematic of Rectifier Circuit with Input and Output Filters

3.3.1 Rectifier Circuit Model in Lumped Parameter System

There are two possible implementations of realizing filters with the above characteristics^{[13],[14]}. Figure 3.8 shows a method with using lumped circuit elements and satisfying these requirements. The elements $L_3, C_3, L_5, C_5, \dots$, form parallel resonant circuits. They are open circuited at the odd harmonics $3\omega, 5\omega, \dots$, respectively. The capacitor C_1 is used for preventing DC flow as well as for series resonating $L_3, C_3, L_5, C_5, \dots$, at the fundamental frequency ω . The $L_2, C_2, L_4, C_4, \dots$, elements in the output circuit are series resonant at the even harmonics $2\omega, 4\omega, \dots$, respectively. The inductance L_o is assumed to be large enough such that the current I_L is mainly DC. In that way the current I_L would consist of a DC plus even harmonics only.

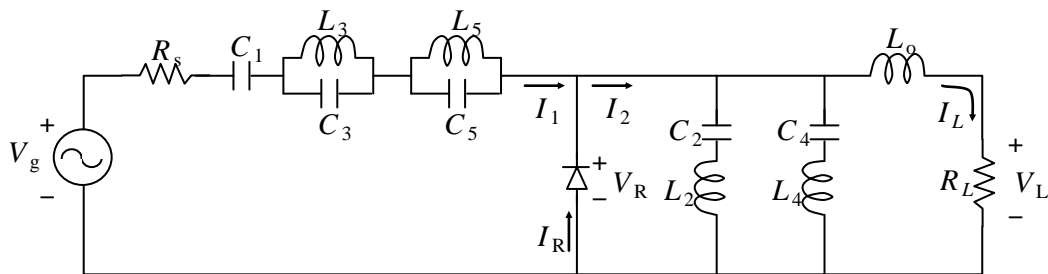


Figure 3.8 Schematic of Rectifier Circuit with Lumped-element Input and Output Filters

Figure 3.9 shows another possible method. In this circuit, the output filter consists of a non-dispersive transmission line terminated in a capacitor C_o in parallel with the load R_L ; it is a quarter wavelength long at the fundamental frequency. When C_o is enough large, the line can be considered to be at the load end and will appear at the diode terminals as an open circuit at $\omega, 3\omega, 5\omega, \dots$ and as a short circuit at $2\omega, 4\omega, \dots$. Since their rectifier circuit analyses are ideal, we adopted the latter circuit design method in this thesis because of its simplicity. Additionally, I used only the capacitance C_1 as the input filter for simplifying and miniaturizing the circuit patterns. Figure 3.10 shows the rectifier circuit pattern and Figure 3.11 is its schematic. It consisted only of a chip condenser, a diode and micro-strip lines printed on the substratum.

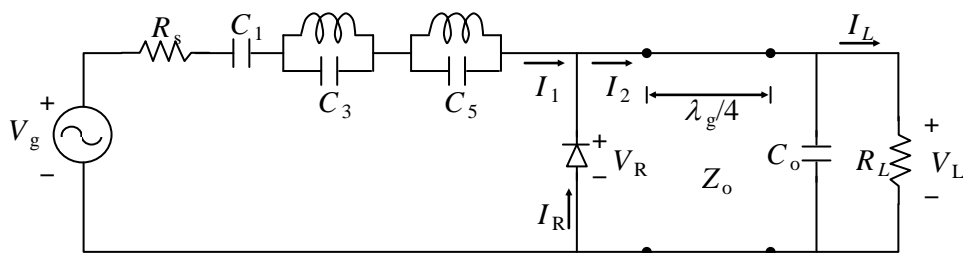


Figure 3.9 Schematic of Rectifier Circuit with a Transmission Line as Output Filter

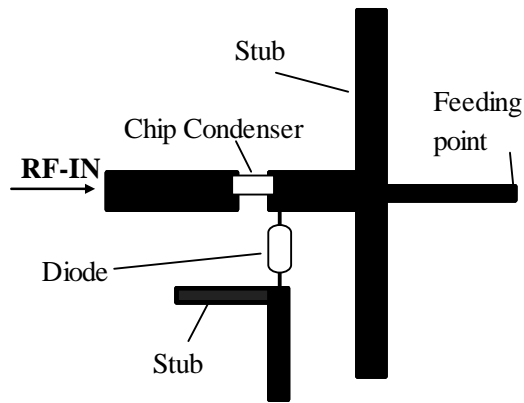


Figure 3.10 Rectifier Circuit Pattern

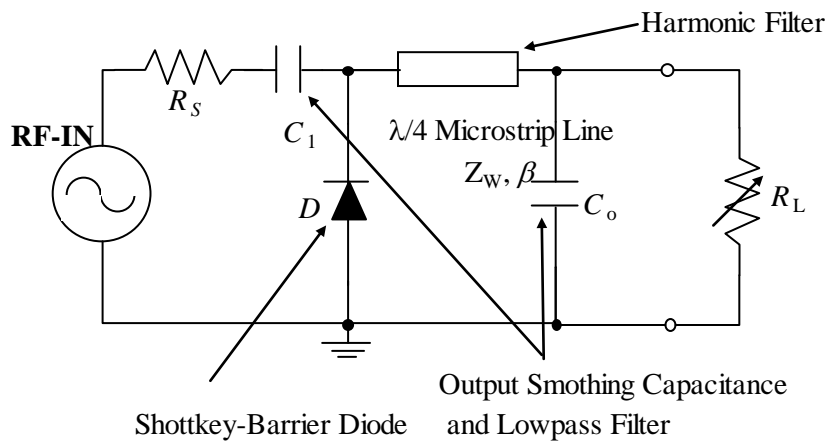


Figure 3.11 Schematic of Rectifier Circuit for Experiment

3.3.2 Matching of Input Impedance

The input line of the rectifier circuit was made as the micro-strip line. The line width W determines the characteristic impedance Z_w of the micro-strip line. (Figure 3.12) Therefore, W is found by Z_w and is expressed as:

$$W = W_0 - \Delta W \quad (3.13)$$

$$W_0 = \frac{8h \sqrt{\left\{ \exp \frac{Z_w \sqrt{\epsilon_r + 1}}{42.4} - 1 \right\}^{7 + \frac{4}{\epsilon_r}} + \frac{1}{\epsilon_r}}}{\exp \frac{Z_w \sqrt{\epsilon_r + 1}}{42.4} - 1} \quad (3.14)$$

$$\Delta W = \frac{t}{\pi} \ln \frac{4e}{\sqrt{\left(\frac{t}{h}\right)^2 + \frac{1}{\pi^2 \left(\frac{W_0}{t} - 0.26\right)^2}}} \quad (3.15)$$

where h is the thickness of the dielectric substrate, t is that of the conductor on the substrate, ϵ_r is the dielectric constant, W_0 is the equivalent width as $t=0$, and ΔW is the offset of it.

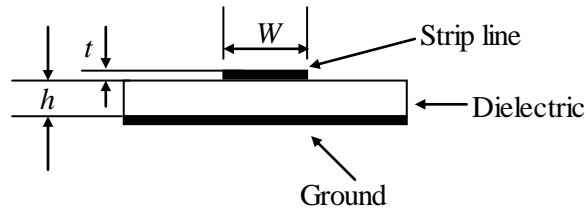


Figure 3.12 Structure of Micro-Strip Line

3.3.3 Design of Stub

In high-frequency circuit, a micro-strip stub with its length $l_s < \lambda_g/4$ plays a role of a capacitor connected in parallel to the circuit^[24]. Figure 3.13 shows the stub pattern and its equivalent circuit. Its capacitance C_{eq} is expressed as:

$$C_{eq} = \left(\frac{1}{Z_C v'_p} - \frac{1}{Z_0 v_p} \right) l_s \quad (3.16)$$

where Z_0 is the impedance of the transmitting line, Z_C is that of the stub, v_p is the phase speed on the transmitting line and v'_p is that on the stub. The phase speeds are also expressed as:

$$\begin{aligned} v_p &= f\lambda_g = \frac{c}{\sqrt{\epsilon_w}} \\ &= \frac{c}{\sqrt{\frac{\epsilon_r + 1}{2} + \frac{\epsilon_r - 1}{2\sqrt{1 + 10h/W}}}} \end{aligned} \quad (3.17)$$

$$\begin{aligned} v'_p &= f\lambda'_g = \frac{c}{\sqrt{\epsilon'_w}} \\ &= \frac{c}{\sqrt{\frac{\epsilon_r + 1}{2} + \frac{\epsilon_r - 1}{2\sqrt{1 + 10h/W_s}}}} \end{aligned} \quad (3.18)$$

where ϵ_w and ϵ'_w are the effective dielectric constants.

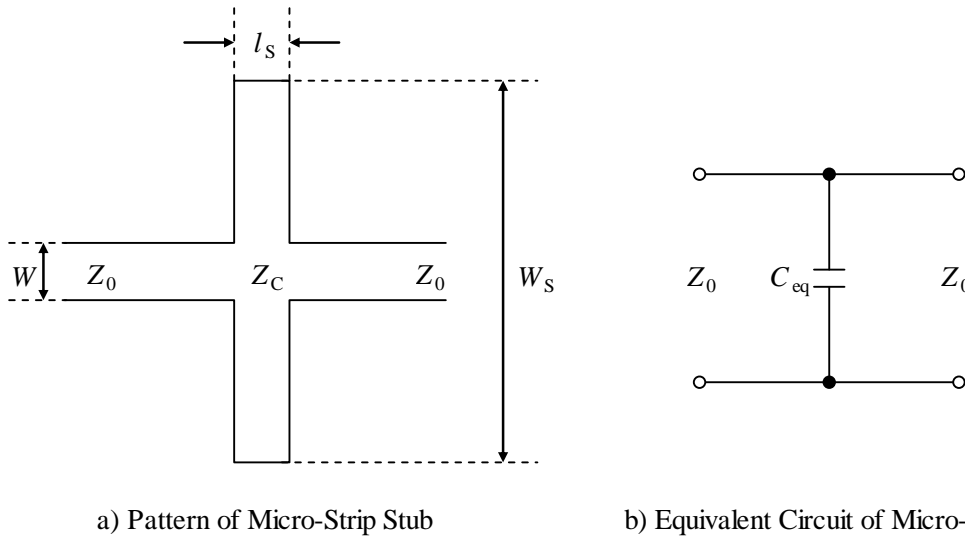


Figure 3.13 Pattern and Equivalent Circuit of Micro-Strip Stub

3.3.4 Output load-line Characteristics

Generally the input power P_a is expressed as^[24]:

$$P_a = \frac{1}{8} \frac{|V_g|^2}{Z_0} \frac{|1 - \Gamma_g|^2}{|1 - \Gamma_g \Gamma_0 e^{-j2\beta l}|^2} \left(1 - |\Gamma_0 e^{-j2\beta l}|^2\right) \quad (3.19)$$

where Γ_0 is the reflection coefficient of the load and Γ_g is that of the power source. Especially when their impedances matched each other, $\Gamma_0=0$ and $\Gamma_g=0$, and then;

$$P_a = \frac{1}{8} \frac{V_g^2}{Z_0} \quad (3.20)$$

Since the circuit matched at $Z_0=50\Omega$, the voltage amplitude V_g of the power source with 10mW of the output power is:

$$V_g = \sqrt{8Z_0 P_a} = 2(V) \quad (3.21)$$

The rectifier circuit analysis is presented below. Since the current $I_1(t)$ is only of the fundamental frequency and $I_1(t)$ consists only of even harmonics, it follows that^{[22], [23]}:

$$V_L = \frac{\pi}{4} V_g - \frac{\pi^2}{8} R_S I_L \quad (3.22)$$

Figure 3.14 shows the characteristic of this equation and indicates follows; from the DC load terminals, the rectifier behave as a DC voltage source of amplitude $(\pi/4)V_S$ and internal resistance $(\pi^2/8)R_S$.

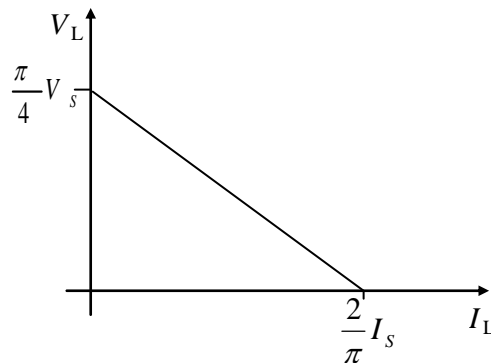


Figure 3.14 Relationship between DC equivalent circuit and load-line

Note that the voltage source is power-level dependent, but the equivalent output resistance is independent of RF power. Using this model, the optimum load for maximum DC load is:

$$(R_L)_{op} = \frac{\pi^2}{8} R_s \quad (3.23)$$

and the maximum dc power output is:

$$(P_L)_{max} = \frac{\left(\frac{\pi}{8} V_s\right)^2}{\frac{\pi^2}{8} R_s} = \frac{V_s^2}{8R_s} \quad (3.24)$$

which gives a 100 percent rectification efficiency.

This ideal efficiency has been achieved because it is assumed no losses in any of the circuit components or in the diode. However, since these losses can be minimized by choosing a rectifier diode with small forward drop and small-series resistance and high- Q circuit elements, the closed-form conversion circuit model would be a good approximation to the characteristics of a high efficiency rectenna element.

Additional factors to be considered are the diode nonlinear depletion layer capacitance and package elements. Figure 3.15 shows the nonlinear V-I characteristic of a diode; the forward current rises steeply over the forward voltage V_f , and the reverse current increases rapidly over the breakdown voltage V_R .

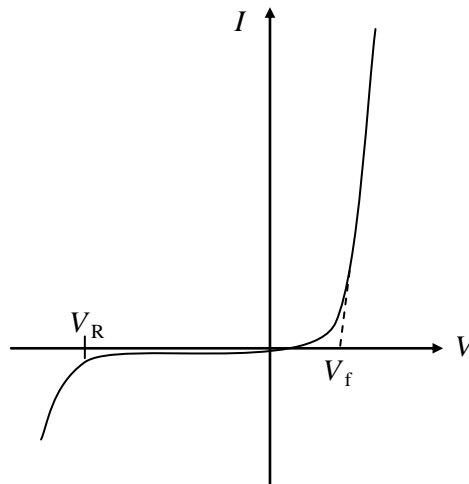


Figure 3.15 V-I Characteristic of Diode

3.3.5 Rectifier Circuit Model in Distributed Parameter System

In order to evaluate the effect of these additional factors, we need a detailed computer simulation model, or distributed parameter circuit model^{[22], [23], [25], [26]}. Figure 3.16 shows the equivalent circuit of a diode in the distributed parameter system. With these equivalent circuits, we could express that rectifier circuit pattern (Figure 3.10) in the distributed parameter system. Figure 3.17 shows the detailed computer simulation model of the rectifier circuit in the distributed parameter system. Although its characteristic was able to be analyzed with general circuit programs, such as SPICE, I could not. It is because the parameters of the diode and the micro-strip lines were not able to be identified; in the high-frequency circuit, the elements induce the capacitances, the reactances and the resistances, and the parameters of diode vary from production lot to production lot, or from element to element. Therefore, I optimized the rectifier circuit pattern from a pre-designed circuit by changing their parameters independently.

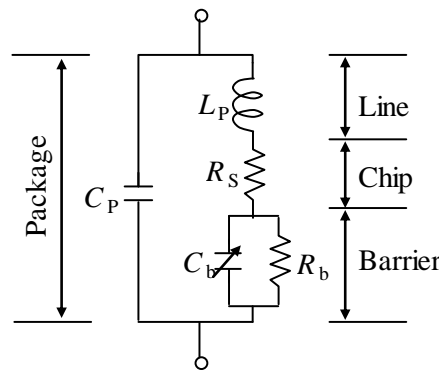


Figure 3.16 Equivalent Circuit of Diode

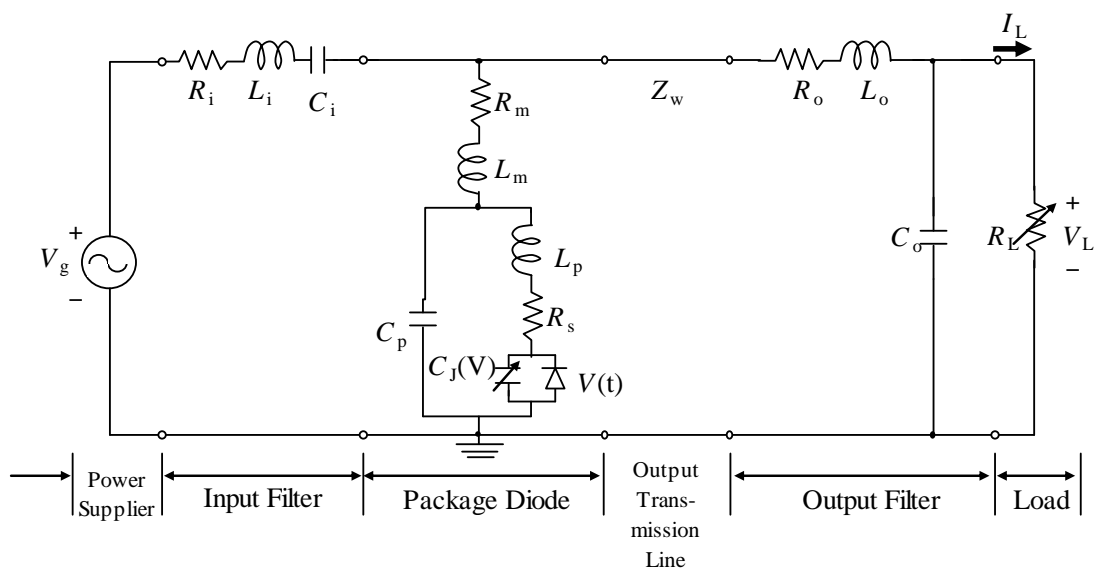


Figure 3.17 Detailed Schematic of Rectifier Circuit for Experiment

Chapter 4

Experimental Apparatus

This chapter shows the power transmission system, the power receiving system and others for the experiments and the demonstration. The power transmission and tracking system was discussed in detail in our past thesis^{[8]-[15]}. The tracking system is abbreviated since the system was also discussed in detail in the past thesis.

4.1 Power Transmission System

Figure 4.1 shows the transmitting array antenna system. Microwave of 5.8 GHz was generated by an oscillator and was divided into five parts by a power divider. The phases of microwave parts without of the middle antenna were changeable individually with using four 6-bit digital phase shifters controlled by a PC. The driver amplifiers returned the power to level before phase shifting. Five FET amplifiers with the output power of 1.0W each massed into totally 5.0W output power.

Figure 4.2 shows the picture of it. Each microwave was guided to an antenna through a semi-flexible coaxial cable. Horn antennas were used as transmitting elements. Figure 4.3 shows the crisscross arranged antenna array; its array pitch d was 110mm and the diameter of the array D was 330mm. The beam was linearly polarized in the y-direction. Table 4.1 shows the specifications of this transmitting system.

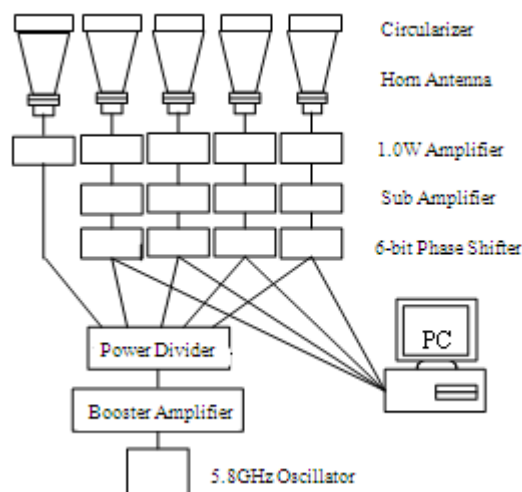


Figure 4.1 Schematic of Transmitting Array antenna System

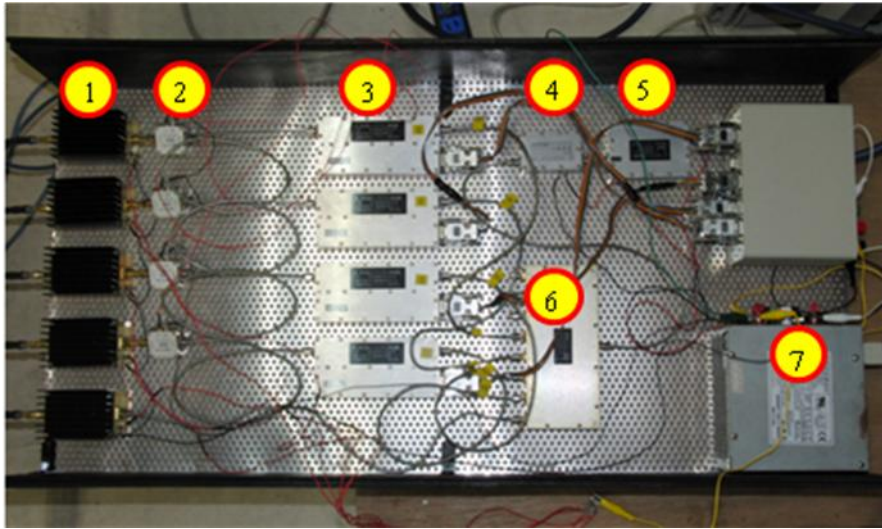


Figure 4.2 Picture of Transmitting System (1: Power Amplifiers, 2: Driver Amplifiers, 3: Phase Shifters, 4: Booster Amplifier, 5: Oscillator, 6: 8 Power Divider, 7: Power Source)

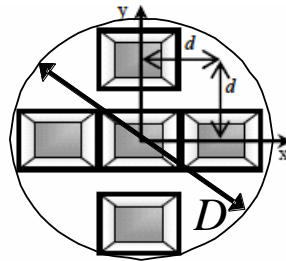


Figure 4.3 Arrangement of five antenna elements of the array

Table 4.1 Specifications of Transmitting Array Antenna System

Microwave Frequency	5.8GHz
Wavelength, λ	51.7mm
Total transmission Power, P	5.0W
Output Antenna	5 Horn antennas
Array pitch, d	110mm ($d/\lambda=2$)
Diameter of the array, D	330mm
Power Source	DC +5V, +12V

4.1.1 Oscillator

Microwave was produced by a oscillator (ArumoTech-OS00T2182) shown in Figure 4.4. Table 4.2 shows its specifications. This oscillator used the plate-tuning method with MOSFET (Metal Oxide Semiconductor Field Effect Transistor) for oscillating. Since it generates about the stable output power of 10 dBm, I used it for evaluating the handmade rectifier circuits by connecting them directly.



Figure 4.4 Picture of Oscillator

Table 4.2 Specifications of Oscillator

Model Name	OS00T2182
Output Microwave Frequency	5.8GHz
Output Power, P_{osc}	+10dBm \pm 2dBm (10mW)
Output Connector	SMA-J
Power Source	DC +12V \pm 0.5V

4.1.2 Power divider

Figure 4.5 shows a power divider (ArumoTech-PD00T2301). Microwave produced by the Oscillator was divided into 8 parts by the power divider, and each output of these parts was 1.25mW. In this experiment, we used five ports as the transmission lines. The unused three output lines were terminated with 50 Ω Terminators for suppressing the effects of the power reflection from one part to the other.

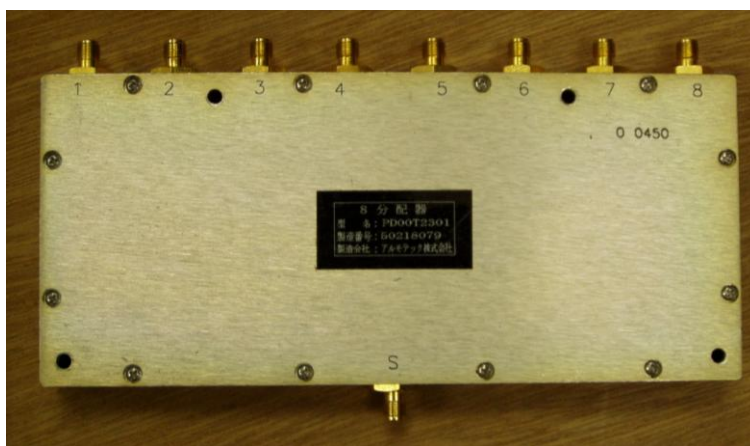


Figure 4.5 Picture of Power Divider

4.1.3 6-bit digital phase shifter

Figure 4.6 shows a phase shifter (ArumoTech-FS01T2150). The output phases are controlled with sending 6-bit signals from a computer to the phase shifters. This device shifted the phase by changing the physical length of the transmission line. Figure 4.7 shows the mechanism of the phase shifting. The phase shifter had the 6 elements each composed of two transmission lines with different length. The difference in length between the upper transmission line and the lower one corresponded to the amount of the shifted phase.

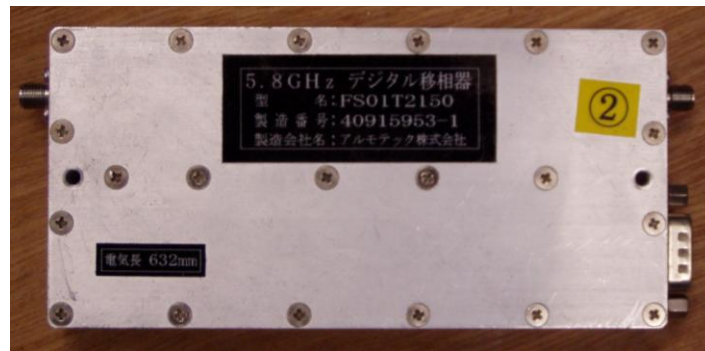


Figure 4.6 Picture of Phase Shifter

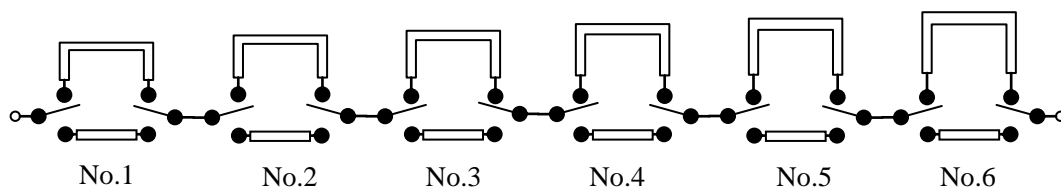


Figure 4.7 Mechanism of phase shifting

4.1.4 Driver amplifier

Figure 4.8 shows a driver amplifier (ArumoTech-AP01T2149). The driver amplifier recovered the power loss generated by the phase shifter. This was set after the phase shifter and before the power amplifier. Table 4.3 shows the specification of the driver amplifier.

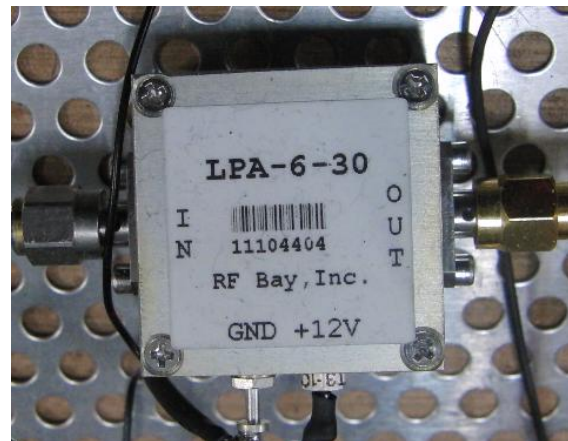


Figure 4.8 Picture of Driver Amplifier

Table 4.3 Specification of the Driver Amplifier

Model Name	AP01T2149
Frequency Range	0.5~6GHz
Output Power, P_{osc}	+30dB or more
Input and Output Connector	SMA-J
Power Source	DC +12V \pm 0.5V

4.1.5 Power amplifier

Figure 4.9 shows a power amplifier (ArumoTech-OS00T2182). It was a FET based amplifier for boosting the signal power to the desired output level finally, about 1.0W. This output power determined the total transmitting power from the horn antennas. The total amount of output power through the power amplifiers was 5.0W.

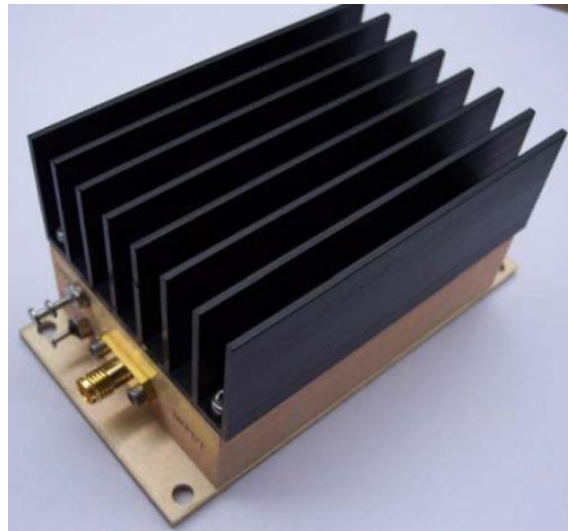


Figure 4.9 Picture of Power Amplifier

4.1.6 Booster amplifier

Figure 4.10 shows a booster amplifier (ArumoTech-AP00T2388). This device installed after the oscillator and before the power divider, and boosted the input power by 4.5dB. Without the booster amplifier, the output power of the power amplifiers often fluctuated due to the differences in phase attenuations at the commanded phases or other unidentified factors. The role of this device was to boost the input power to the power amplifiers enough for them to be reliably saturated. Table 4.4 shows the specification of the booster amplifier.

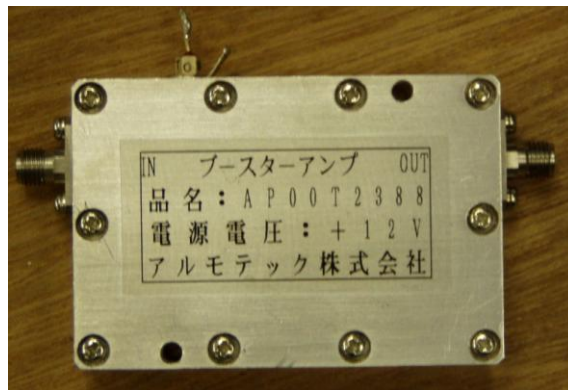


Figure 4.10 Picture of Booster Amplifier

Table 4.4 Specification of Booster Amplifier

Model Name	AP00T2388
Frequency Range	5.8GHz
Amplifier Gain	4.5dB (at 10mW input)
Input and Output Connector	SMA-J
Power Source	DC +12V \pm 0.5V

4.1.7 Horn antenna

Figure 4.11 shows the picture of a horn antenna. Its input plane size was $\Delta x=40\text{mm}$ and $\Delta y=20\text{mm}$ exit plane size was $\Delta x=110\text{mm}$ and $\Delta y=81\text{mm}$. The select of the antenna type for transmission mainly depended on two factors: the gain (or directivity) of the antenna and its polarization characteristics. Since the target had only a limited area available for receiving the transmitted energy, a high directivity of an antenna was desirable. Two prerequisites were needed for a high directivity. One was a large effective aperture size and the other was a uniform phase front at the aperture plane. The uniformity of the phase front also had an indirect effect on the aperture size and therefore on the directivity. The absolute gain G_a of a horn antenna was expressed as:

$$G_a = 10 \log \left(\frac{4\pi \Delta x \cdot \Delta y}{\lambda^2} \right) \times \eta \quad (4.1)$$

where the aperture efficiency was 0.8 and the aperture size A_e was $0.11 \times 0.081 = 0.00891 \text{ m}^2$. This gives the G_a of this thesis was about 15.17dBi.

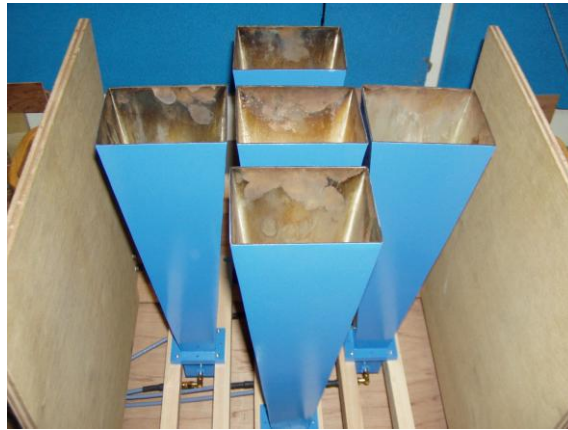


Figure 4.11 Picture of Horn-Antenna

4.1.8 Circularizer

Figure 4.12 shows the picture of a circularizer. It changes a linear polarized wave which generated by the horn antenna to a circular polarized wave. This allows the transmission system to be a polarity-free transmission system.

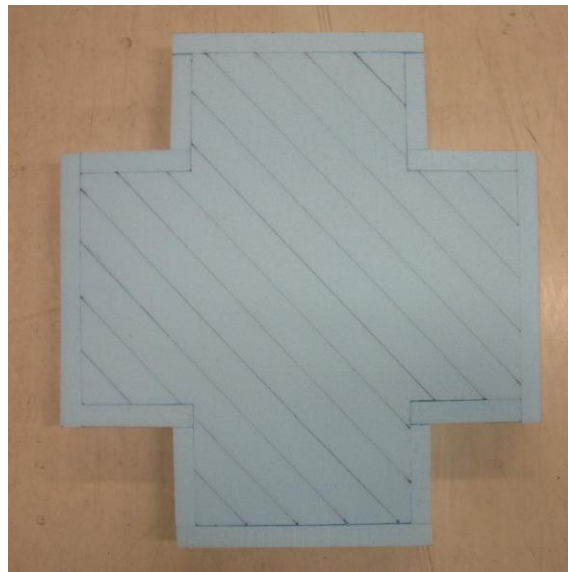


Figure 4.12 Picture of Circularizer

4.2 Power Receiving System / Measurement Apparatus

Figure 4.13 shows the power receiving system. It composed of antennas, rectifiers, a resistor, a power sensor, a power meter, and a digital multi meter. The microwave transmitted by the power transmitting system was received by the antennas and the rectennas. In (a), the microwave received the antennas was measured by the power sensor and the RF power was outputted by power meter. In (b), the microwave received the rectennas was converted to DC power by the rectifiers of the rectennas, was loaded by the adjustable resistor and was measured as the output voltage by the digital multi meter.

Figure 4.14 shows the characteristics measurement system of the antenna or the rectifier circuit. In (i), the antenna was connected to a network analyzer and measured its characteristics such as the return loss and the impedance. In (ii), the microwave transmitted by oscillator was converted to DC power by the circuit, was loaded by the adjustable resistor and was measured as the output voltage by the digital multi meter.

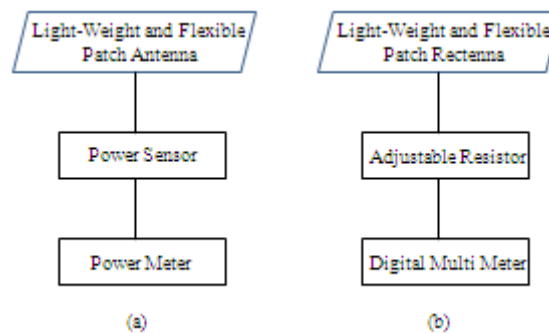


Figure 4.13 Schematic of Power Receiving System

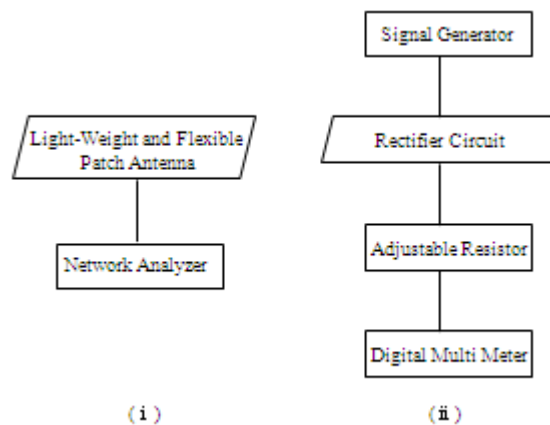


Figure 4.14 Schematic of Characteristics Measurement of the Antenna and Rectifier Circuit

4.2.1 Light-Weight Flexible Patch Antenna / Rectenna

Figure 4.15 show a light-weight flexible patch antenna and rectenna I developed. I used a felt pad as the dielectric and a copper tape as the conductor. This is referenced by the wearable patch antenna developed by Tanaka et al. in NICT^[27]. Figure 4.16 shows the schematic of the antenna and Table 4.5 shows the specification. The antenna's and rectenna's characteristics were described in detail in chapter 5.

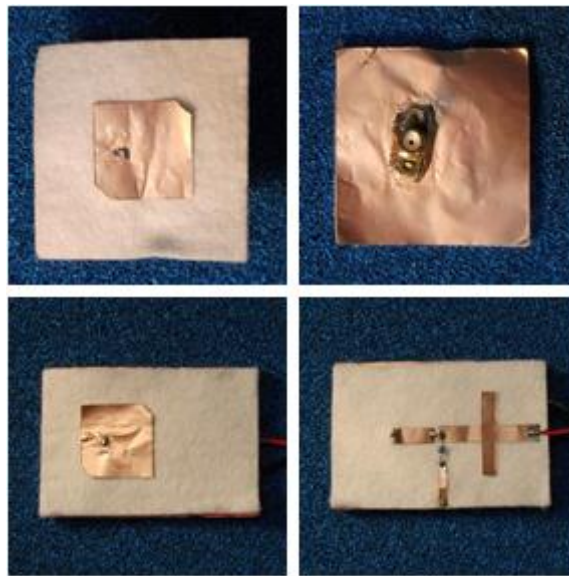


Figure 4.15 Picture of Light-Weight Flexible Patch Antenna and Rectenna

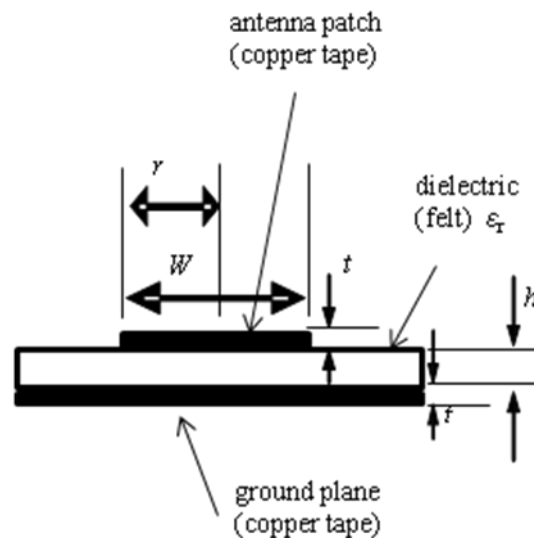


Figure 4.16 Schematic of Antenna

Table 4.5 Specification of the Antenna

Parameters	Values / Product
copper tape	TERAOKA No.831S
Felt	Wool 60% and Rayon 40%
copper tape thickness h [mm]	0.07
dielectric thickness [mm]	1.0

4.2.2 Power Sensor and Power Meter

Figure 4.17 and Figure 4.18 show the power sensor and the power meter (HP 437B and 8481A) for measurement of high frequency RF power.



Figure 4.17 Picture of Powere Sensor (HP 437B)



Figure 4.18 Picture of Power Meter (HP 8481A)

4.2.3 Adjustable Resistor

Figure 4.19 shows a resistor. It had the range 1 - 500 Ω . We were able to measure the loaded output voltage V_L (Figure 4.20).



Figure 4.19 Picture of Adjustable Resistor

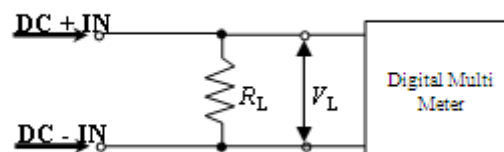


Figure 4.20 Schematics of Circuit of Measurement of the Loded Output Voltage

4.2.4 Digital Multi Meter

Figure 4.21 shows a digital multi meter (kaise KU-1188). It displayed the loaded output voltage.



Figure 4.21 Picture of Digital Multi Meter (kaise KU-1188)

4.2.5 Signal Generator

Figure 4.22 shows a Signal Generator (Hittite HMC-T2000). It is an electronic device that generates repeating or non-repeating electronic signals.



Figure 4.22 Picture of Signal Generator (Hittite HMC-T2000)

4.2.6 Network Analyzer

Figure 4.23 shows a Network Analyzer (HP 8722D). It is an instrument that measures the network parameters of electrical networks. Network analyzers commonly measure S-parameters because reflection and transmission of electrical networks.

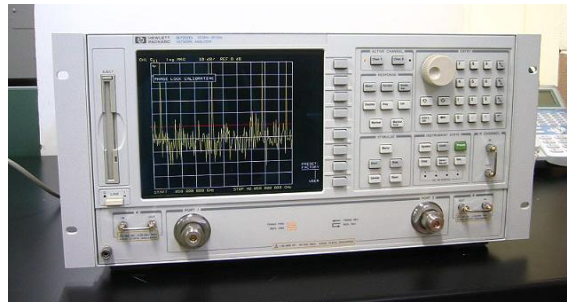


Figure 4.23 Picture of Network Analyzer (HP 8722D)

4.3 Experimental Setup and Demonstration

We measured on a mounting structure surrounded by flat tile ferrite absorber. Additionally, we made a MAV model. In this section, I describe about the mounting structure and the others for experimenting or demonstrating.

4.3.1 Mounting structure

Figure 4.24 shows a mounting structure for the measurement system. It was made of wood and thermoplastics. The framework was surrounded by flat tile ferrite absorber for reducing the reflection effect. The movable ranges were: $x: \pm 450[\text{mm}]$, $y: \pm 450[\text{mm}]$, $z: 0 \sim 2000[\text{mm}]$.

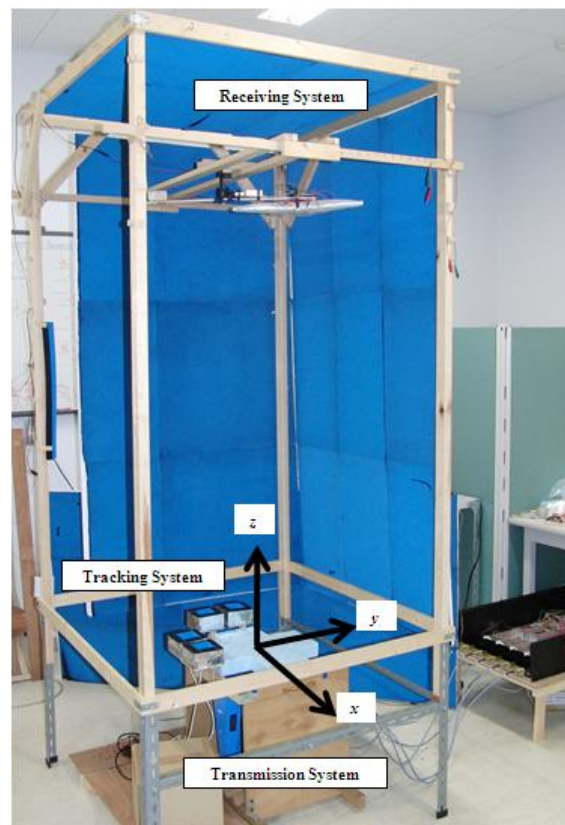


Figure 4.24 Picture of Mounting Structure

4.3.2 Electrical Motor for MAV Model

Figure 4.25 shows an electrical motor for the power transmission demonstration and Table 4.6 is its specification. Since it was able to operate with low electric power, it was adopted for the demonstration.

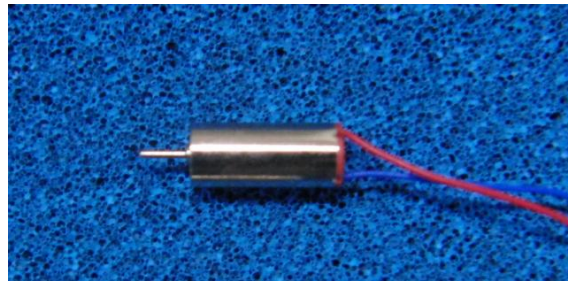


Figure 4.25 Picture of Electrical Motor

Table 4.6 Specification of the Motor

Parameters	Values
Min. Operating Voltage V_{\min} [mV]	100
Min. Operating Current I_{\min} [mA]	1
Inertial Resistance R_L [Ω]	4
Rated Voltage V_{rat} [V]	3.7
Rated Current I_{rat} [mA]	60

4.3.3 MAV Model and Demonstration

Figure 4.26 shows a MAV model and Table 4.7 is its specification. The small rectennas are 5.8GHz rectennas for the receiving system, the large one is 2.45GHz antenna for the tracking system which transmit a pilot signal to the transmission system. When the power received and rectified by the rectennas flows to the electrical motor, the motor moves. Figure 4.27 shows the picture of the rectennas on the MAV model. Because of the rectennas's flexibilities, they are able to be mounted along the MAV's curved surface.

Figure 4.28 shows an experimental setup for the demonstration. The MAV model is mounted on a supporting bar. 12V batteries and a 2.45GHz oscillator used for the tracking system are also mounted on the bar. On the center of the bar, there is a motor and it moves the bar circularly. Therefore the MAV also moves circularly. The MAV position is detected by the tracking system and microwave beams are transmitted to the MAV by the transmission system automatically.

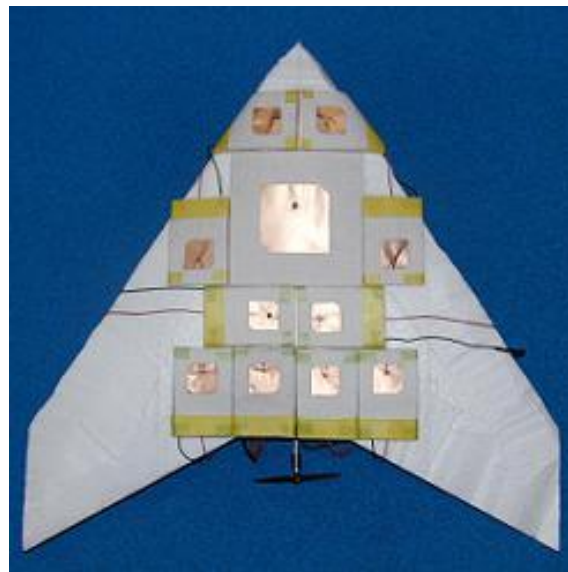


Figure 4.26 Picture of MAV model

Table 4.7 Specification of MAV model

Components / Parameters	Pieces / Values
2.45GHz Antenna for Tracking	1
5.8GHz Rectenna	10
Electric motor	1
Total weight [g]	103



Figure 4.27 Picture of the Rectennas on the MAV model

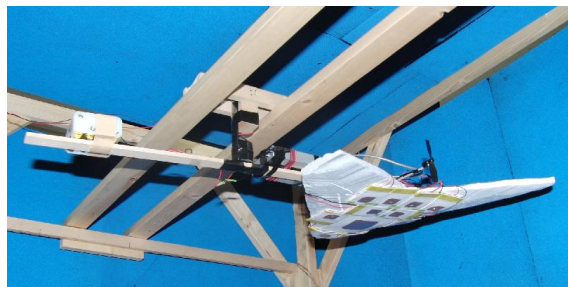


Figure 4.28 Picture of the MAV Demonstration Setup

Chapter 5

Measurement Results and Discussions

This chapter shows the measurements results of the experiments and discussions about the light-weight flexible patch antennas, the RF-DC conversion circuit patterns, the rectenna and the demonstration with the rectenna array.

5.1 Antenna Measurement

5.1.1 Dielectric Constant

The dielectric constant of felt pad was measured before I developed the light-weight and flexible antenna. It is important for making antennas to grasp the dielectric constant. This is because the size of antenna is determined by the dielectric constant and the wave length. In this research, I used felt pad as the dielectric. Then, I made some size pattern of antenna by using a reference to linear-polarized antenna and each resonance frequency were measured by the network analyzer. Finally I calculated each dielectric constant using in (3.1). Figure 5.1 shows the antenna I made.

Table 5.1 shows the result of measurement of each resonance frequency. It was found that the resonance frequency decreased by about 0.3 ~ 0.5 GHz with increasing the antenna size. I calculated the dielectric constant of the felt pad and it was found that the constant was 1.003. So I made a circular-polarized wave antenna and Figure 5.2 shows the picture of the antenna and Table 5.2 shows the size.

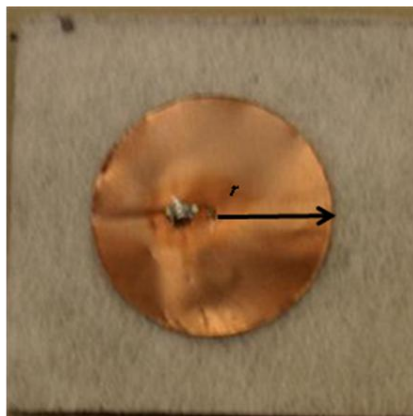
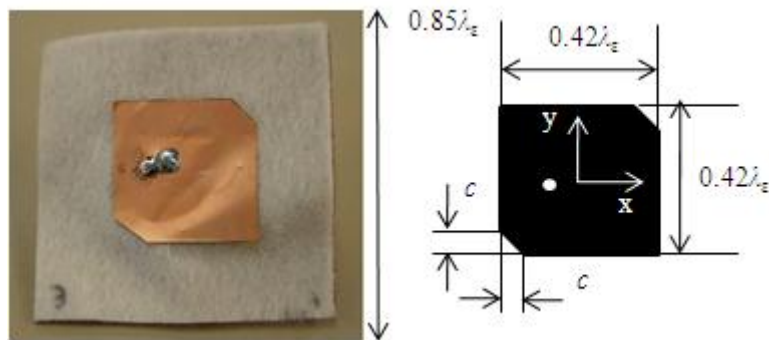


Figure 5.1 Picture of Liner-Polarized Wave Antenna

Table 5.1 Return Loss and Resonance Frequency of Antennas

radius: r [mm]	Return Loss [dB]	Resonance Frequency [GHz]
9.5	-30	8.05
10.0	-12	7.39
10.5	-20	7.11
11.0	-15	6.81
11.5	-25	6.48
12.0	-22	6.24

**Figure 5.2 Picture of Circular-Polarized Wave Antenna and Antenna Size****Table 5.2 Specifications of Circular-Polarized Wave Antenna**

Parameters	Values
Dielectric constant: ϵ_r	1.003
Wave length in the felt pad: λ_e [mm]	51.6
Size of the felt pad [mm]	$0.85\lambda_e \times 0.85\lambda_e$
Size of the copper tape [mm]	$0.42\lambda_e \times 0.42\lambda_e$
Size of the cutout: c [mm]	c
Feeding point: ρ [mm]	$-x$ axis 4.0

5.1.2 Dependence of Yaw-Angle

I made the two types of antenna such as a liner polarized antenna and a circular polarized wave antenna and measured the polarized wave properties of the antennas. In this research the circular polarized antenna was an ACPW (Figure 5.2) and the linear polarized antenna was a circle antenna (Figure 5.1). Their feedings were a behind pin's feeding method for simply.

The result is shown in Figure 5.3 The c means the cutout size of the ACPWs. The transmitting microwave is circular polarized wave. So the linear polarized wave antenna is average 50% efficiency in theory. The result corresponds to the theory. In contrast, the circular polarized wave antenna is 100% efficiency in theory. However the antenna ($c=3\text{mm}$) was average 70% and the other antenna ($c=4\text{mm}$) was average 50% efficiency in the experiment. It is assumed that the polarized properties of the receiving antennas weren't consistent with that of the transmission antennas. Therefore the polarized wave efficiency is able to be improved by an agreement with the polarized properties of transmission antennas.

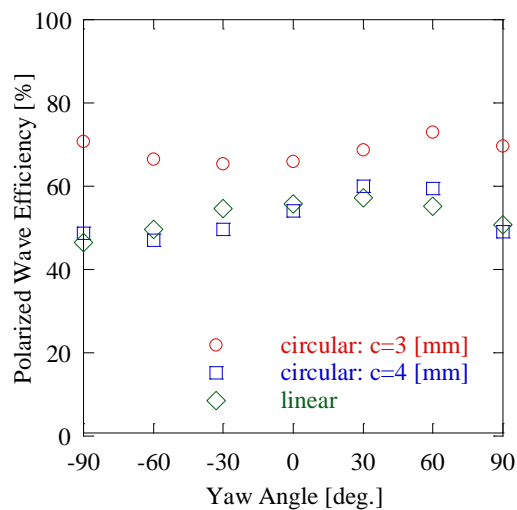


Figure 5.3 Polarized Wave Properties

5.1.3 Characteristic of Antenna (Return Loss)

Figure 5.4 shows the result of return loss measurement of the light-weight and flexible antenna by the network analyzer. I also measured the return loss when the antenna was bent as Figure 5.5 in case of a mounting on MAV. The result is shown in Figure 5.6. In Figure 5.6, 0 deg. means no bending, 45 deg. means a 45-degree bending and a 90 deg. means 90-degree bending for the E-plane. The return loss was about -20 dB with no bending and the resonance frequency was 5.8 GHz. The resonance frequency increased by about 0.25 GHz for 45-degree bending. Table 5.3 shows the return loss at 5.8 GHz. At 5.8 GHz, the return loss increased by 10dB for 45-degree bend and by 12dB for 90-degree bend. In fact the efficiency decreased by 5% for 45-degree bend and by 14% for 90-degree bend.

It is found that, in the measurement, the antennas using the felt pad as the dielectric were not inferior to the regular antennas using hard dielectrics. Since, in generally, the antennas are not used with a bend of 90-degree, the antennas with a bend within 45-degree are enough to be used in practice.

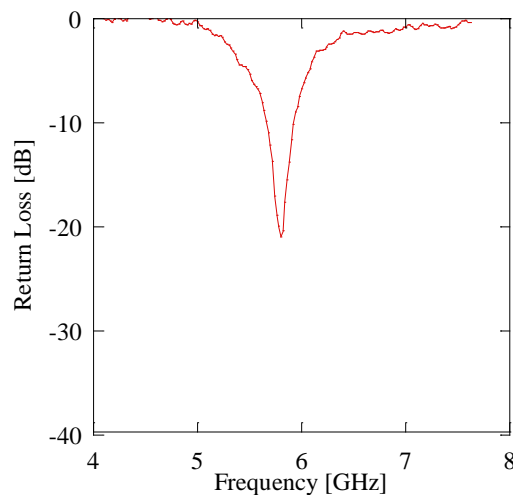


Figure 5.4 Return Loss of the Light-Weight Flexibel Antenna

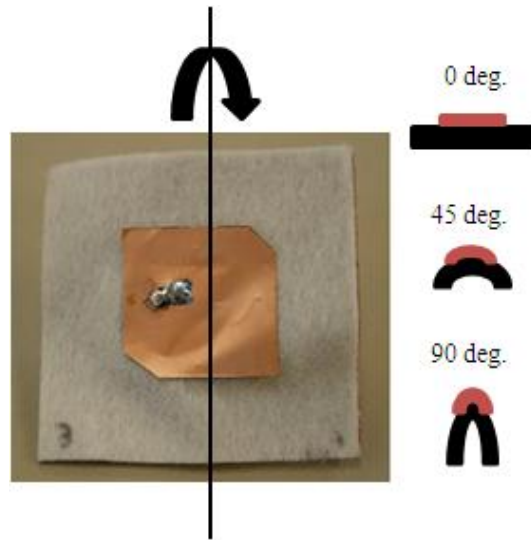


Figure 5.5 Picture of Antenna and Bend Definition

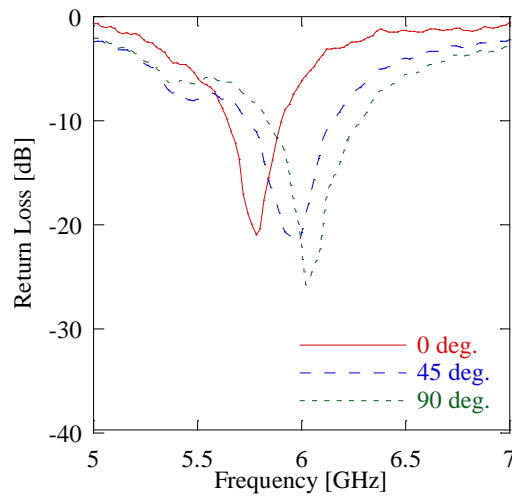


Figure 5.6 Bending Properties of the Light-Weight Flexible Antenna

Table 5.3 Bending Properties and Efficiency of the Light-Weight Flexilbe Antenna

Parameters	0 deg.	45 deg.	90 deg.
Return Loss [dB]	-20.3	-12.3	-8.31
Efficiency [%]	99	94	85

5.2 RF-DC Conversion Circuit Measurement

In designing rectifier circuit patterns, variable parameters are below:

- Type of Schottky Barrier Diode (SBD): D
- Capacitance of chip condenser: C_0
- Input width: W
- Input length: l_{in}
- Width between diode and ground: W_g
- Length between diode and ground: l_g
- Output transmission line (OTL) length: l_{tl}
- Low Pass Filter (LPF) shape: W_C, l_C
- Output width: W_{out}
- Output length: l_{out}

Figure 5.7 shows their parameters on the pattern. The parameters of W, l_{tl} are predetermined by the theory; $W=3.82\text{mm}$ at 5.8GHz for impedance matching, and $l_{tl}=\lambda_g/4$ for output filter. Moreover, it was founded by the past research in our laboratory that some parameters seldom affect the conversion efficiency; $C_0, l_{in}, W_g, W_C, l_C, W_{out}$ and l_{out} . First I designed the standard rectifier circuit patterns. Table 5.4 shows its values and products. I experimented with varying the parameters independently and discuss the results below.

In following experiments, I connected the test rectifier circuit to the oscillator directly, and I measured the output voltage $V_{measured}$ from the rectifier circuit with the digital multi meter. The wattage $P_{measured}$ of the load is expressed as:

$$P_{measured} = \frac{V_{measured}^2}{R_L} . \quad (5.1)$$

where R_L is the resistance value of the load. Since the input power P_{in} is given as 13.2mW from the oscillator specification, the conversion efficiency of the rectifier circuit is found by:

$$\eta = \frac{P_{measured}}{P_{in}} . \quad (5.2)$$

Thus, I calculated the efficiencies with changing the parameters.

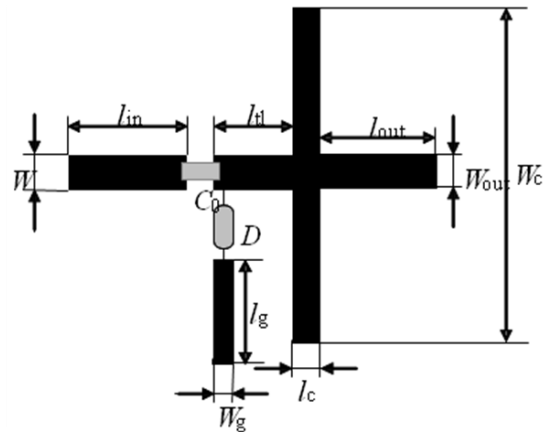


Figure 5.7 Schematic of Rectifier Circuit Pattern Parameters

Table 5.4 Parameters for Standard Rectifier Circuit Pattern

Parameters	Value / Product
D	1SS97 (NEC)
C_0 [pF]	100
W [mm]	3.82
l_{in} [mm]	12.9 ($\lambda_g/4$)
W_g [mm]	1.50
l_g [mm]	12.9 ($\lambda_g/4$)
l_{tl} [mm]	12.9 ($\lambda_g/4$)
W_C [mm]	25.00
l_C [mm]	3.00
W_{out} [mm]	1.00
l_{out} [mm]	12.9 ($\lambda_g/4$)

5.2.1 Capacitance of Chip Condenser: C_0

The role of the chip condenser was smoothing the DC and preventing it from flowing to the RF input side. In these reasons, the chip condenser was acceptable if it had a certain value about over 1pF. I used the following values and experimented; 33pF and 100pF. Figure 5.8 shows the conversion efficiency related to the capacitance of the chip condenser. As seen in the figure, the conversion efficiency is related to the capacitance values.

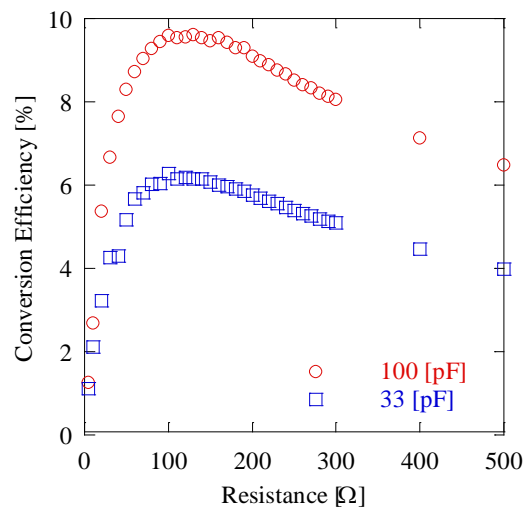


Figure 5.8 Load Characteristic related to Capacitance of Chip Condenser

5.2.2 Length of Diode and Ground: l_g

It was found, in our past research, that the length of diode and ground (D-G length) is very important parameter. Figure 5.9 shows the result for changing D-G length. It is seen that a maximum value of the conversion efficiency is reached at $\lambda_g/4$. So I discuss the effect from two view points.

Firstly, it seems that the effect is attributed to the input voltage to the diode. In antenna theory, when the transmission line length is $\lambda_g/4$, the voltage of the end of the transmission line reaches a peak. The diode characteristics become better when the applied voltage is larger. Therefore, it is assumed that the efficiency comes to a maximum.

Secondly, it seems that the effect is associated with the input impedance. Since one end terminal is connected to the ground, $Z_L=0$, and the equation (2.37) is represented as:

$$Z_{in} = Z_0 \frac{Z_L + jZ_0 \tan \beta l}{Z_0 + jZ_L \tan \beta l} = jZ_0 \tan \beta l = \begin{cases} \infty & \left(l = \frac{\lambda_g}{4} + n \times \frac{\lambda_g}{2} \right) \\ 0 & \left(l = (n+1) \times \frac{\lambda_g}{2} \right) \end{cases}. \quad (5.3)$$

Where the point locates from the shorted end terminal by $Z_{in}=\infty$, and the circuit is opened at the point. Moreover, the point does by $Z_{in}=0$, and the circuit is shorted. However, in this experiment, the efficiency comes to the maximum near $\lambda_g/4$. It is because the effect of the lead line length of the diode package end to the D-G line junction is so large that the lead line length influences on the D-G line^[28].

From above two view points, it is found that the D-G lines are necessary to be determined with respect to each diode.

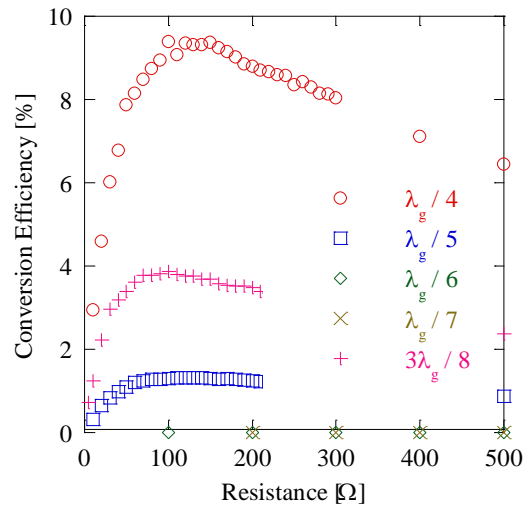


Figure 5.9 Load Characteristic related to D-G length

5.2.3 Pieces Number of the Low Pass Filter

The low pass filters take a stub's role in the circuit which discussed in Chapter 3. Figure 5.10 shows two types of the circuit, one has 1 LPF and the other has 2 LPFs. The conversion efficiency of each circuit is shown in Figure 5.11. It was found that the efficiency of the circuit which had 2 LPFs was higher by 2% than the other which had 1 LPF. It is because the effect of the filter goes up when the pieces number increases. However the size of the circuit is larger when the number is bigger. In case of a mounting on MAV as a rectenna array, larger circuit is not suitable. Therefore the best pieces number of LPF is defined as 1 in this thesis.

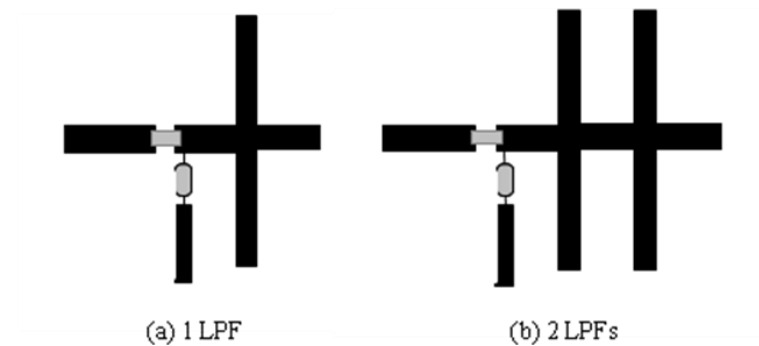


Figure 5.10 Schematic of Rectifier Circuit Pattern

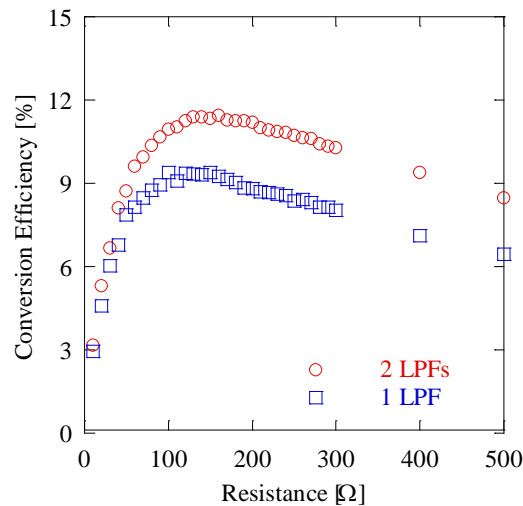


Figure 5.11 Load Characteristic related to Number of LPFs

5.2.4 Input Line Width: W

The input line width was calculated as 3.82mm by the equation (3.13) - (3.15). Although it is the determined parameter for impedance matching as 50Ω , the impedance of the antennas I developed was not 50Ω but 30Ω . Therefore the input width was recalculated as 4.65mm.

Figure 5.12 shows the effect from the width difference. As seen in this graph, the efficiency of the width, 4.65mm, is larger than the other one. It is because the impedances of the antenna and the circuit are matched sufficiently.

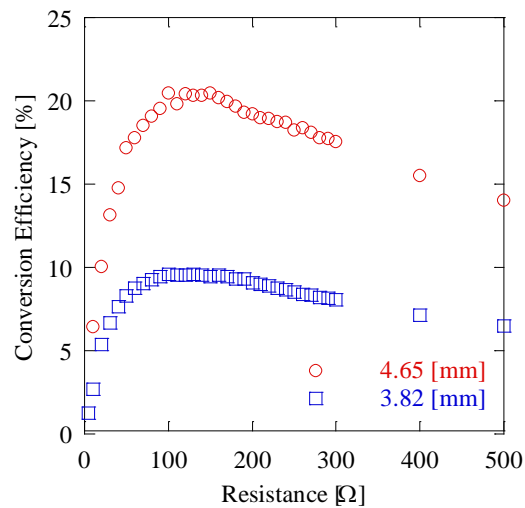


Figure 5.12 Load Characteristic related to Input Line Width

5.2.5 Diode Variations: D

The diode parameters are important for the circuit, in particular, the forward voltage, the inverse voltage and the electrostatic capacity. Lower forward voltages make the current be larger and lower electrostatic capacities make the leak current be smaller^[29]. Table 5.5 shows the specifications of four types of diode and Figure 5.13 shows the result when the diode was changed in various ways.

5082-2035, compared to 1SS97, is larger efficiency because of its advantage of the forward voltage. However 1SS315 and HSM88WA are smaller efficiency in comparison with 5082-2035 though their diode parameters are advantageous. It is assumed that, since their sizes are different from the 5082-2035 and 1SS97, the optimized D-G length values are not equal to $\lambda_g/4$. Therefore, it is important to optimize the D-G length with respect to each diode, which discussed in section 5.2.3 as well.

Table 5.5 Specifications of four Diodes

Parameters	5082-2035 (Avago)	1SS97 (NEC)	1SS315 (TOSHIBA)	HSM88WA (RENESAS)
Size [w :mm \times l :mm]	1.5×4	1.5×4	1×1.5	3×1.5
Forward voltage [V]	0.34	0.50	0.25	0.42
Inverse voltage [V]	8	10	5	10
Electrostatic capacity [pF]	1.0	1.0	0.6	0.85

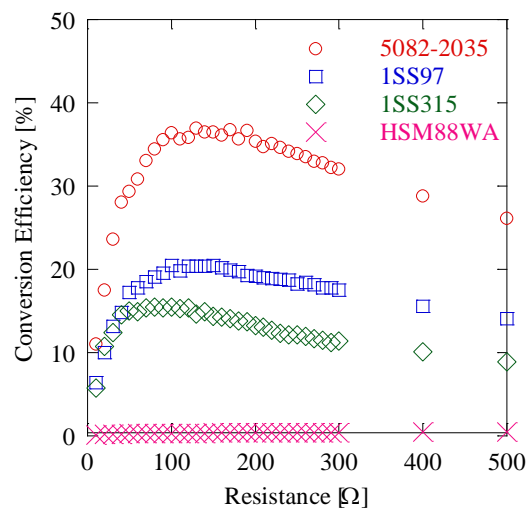


Figure 5.13 Load Characteristic related to Diode

5.2.6 Redesign of Rectifier Circuit

Based on the above results, I redesigned the rectifier circuit. Table 5.6 shows the redesigned parameters. Figure 5.14 shows the effect of redesigning. As a result, the conversion efficiency of the new designed circuit was improved in comparison to the pre designed circuit.

Table 5.6 Parameters of New Design Rectifier Circuit Pattern

Parameters	Value / Product
D	5082-2035 (Avago)
C_0 [pF]	100
W [mm]	4.65
l_{in} [mm]	12.9 ($\lambda_g/4$)
W_g [mm]	1.00
l_g [mm]	12.9 ($\lambda_g/4$)
l_{tl} [mm]	12.9 ($\lambda_g/4$)
W_C [mm]	25.00
l_C [mm]	3.00
W_{out} [mm]	1.00
l_{out} [mm]	12.9 ($\lambda_g/4$)

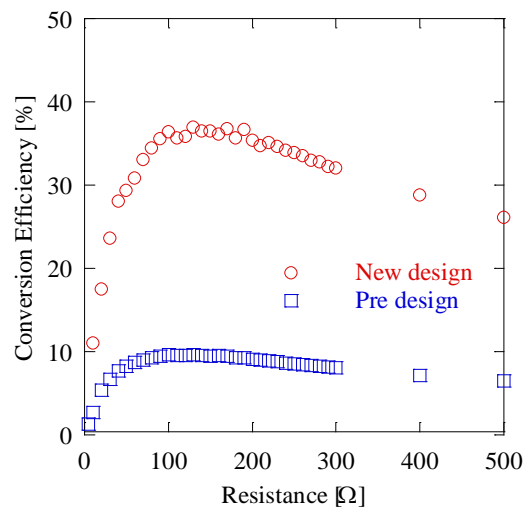


Figure 5.14 Load Characteristic of New and Pre design

5.2.7 Bending Properties

In case of a mounting on the MAV model which has curved surface, the RF-DC circuit was measured with some degree bend. Figure 5.15 shows the picture of the circuit and the definition of A and B plane. The bending properties result is shown in Figure 5.16. The conversion efficiency shows no change with B-plane bend. In contrast, the efficiency with A-plane bending decreases followed by the bend degree. It is because, since there was the D-G line on the A-line, the D-G length was changed relatively by the bend and the D-G length strongly influences on the efficiency. Therefore, the bend directions are important when the circuit is mounted on the MAV model.

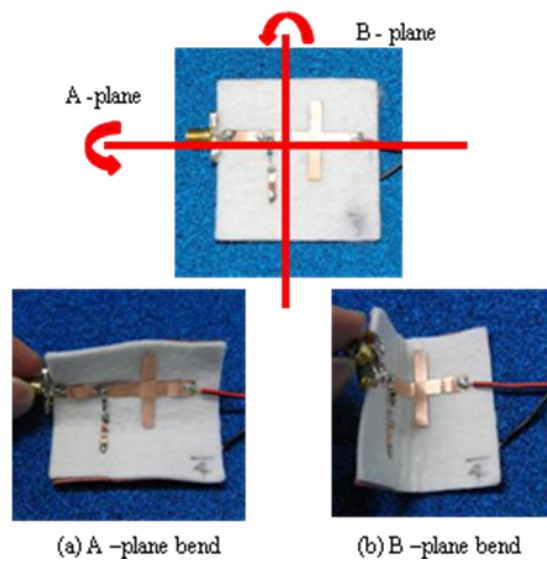


Figure 5.15 Pictures of the Circuit and Bending definition

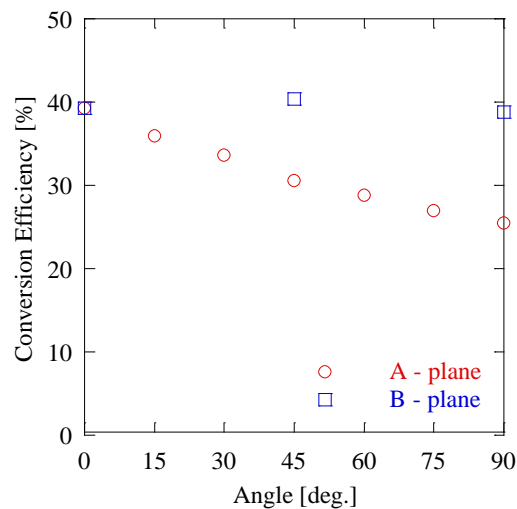


Figure 5.16 Bending Properties of the Light-Weigh Flexible RF-DC Conversion Circuit

5.2.8 Dependence of Input Power

Generally, input power to diode is larger and the efficiency is higher in small power range (Figure 3.1b). Figure 5.17 gives the dependence on the input power. As can be seen from the graph, the conversion efficiency increases with increasing the input power and there is a peak of the efficiency, 58%, at 60mW. It is not inferior to the regular RF-DC circuits on hard dielectric boards. Therefore, it is found that the RF-DC conversion circuits on the light-weight flexible dielectric are particularly useful for the mounting on the MAV.

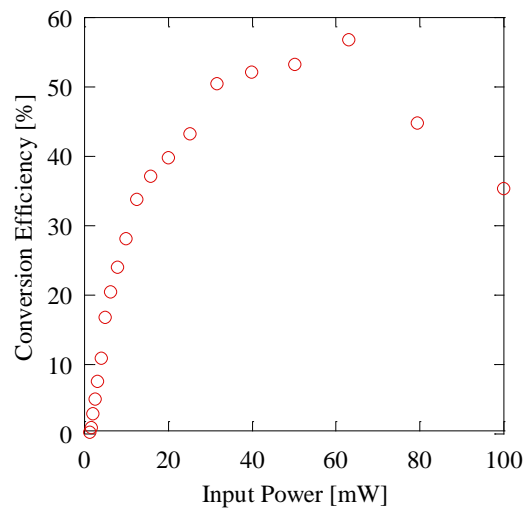


Figure 5.17 Conversion Efficiency related to Input Power

5.3 Rectenna Array Measurement

5.3.1 Optimization of Array Pitch

When an input power to rectennas is larger, the input voltage exceeds the breakdown voltage of the diode and the RC-DC conversion circuit is not able to work well as a rectifier circuit. Therefore the input power to rectennas is limited. Then, in practice, some rectennas are arrayed for power increasing to loads. I measured RF power of just the central rectenna in the arrangement (Figure 5.18) with changing array pitch: p and compared with the RF power of one rectenna not arrayed. And I calculated the optimum arrayed pitch of the rectenna array. The result is shown in Table 5.7. From Table 5.7, the receiving RF power decreases with decreasing the array pitch. This is because the rectenna robs each other of RF power in space. As a result, it is found that the optimum array pitch is 0.85λ . However the receiving efficiency declines by 10% compared with one element of the rectenna.

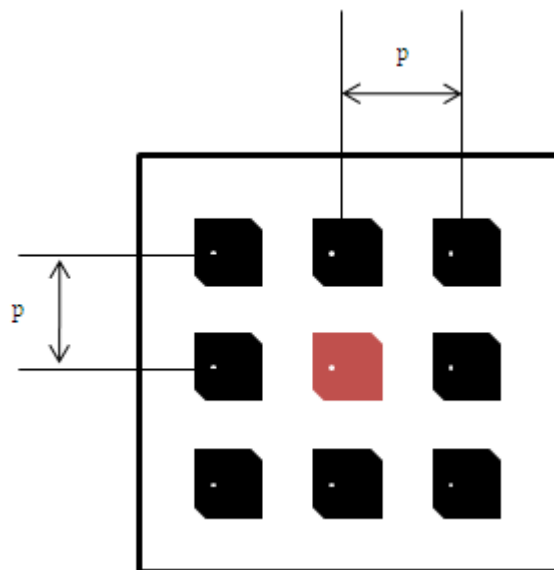


Figure 5.18 Schematic of Rectenna Array Pitch

Table 5.7 Measurement Result of each array pitch

p [mm]	0.65λ	0.70λ	0.75λ	0.80λ	0.85λ	0.90λ
$P_{array,center} / P_1$	0.08	0.30	0.34	0.36	0.90	0.93
$\frac{P_{array,center} / p^2}{P_1 / \lambda^2}$	0.19	0.61	0.60	0.56	1.24	1.14

5.3.2 Two Antenna Elements for One Rectifier Circuit

The efficiency of the RF-DC conversion circuit is larger with the higher input power. Then, two antenna elements were applied to one rectifier circuit in order to increase the input power. Figure 5.19 shows the picture of the rectenna which has two antennas and one rectifier circuit, and Table 5.8 gives the result of comparison to the rectenna which has one antenna and circuit. As can be seen from the table, the rectenna which had two antennas and one circuit was inferior to the other one. It is because that the microwave radiated and reflected on the transmission line, and two input microwave negated each other due to their phase difference. Therefore, it is difficult to apply some antennas to one RF-DC conversion circuit.

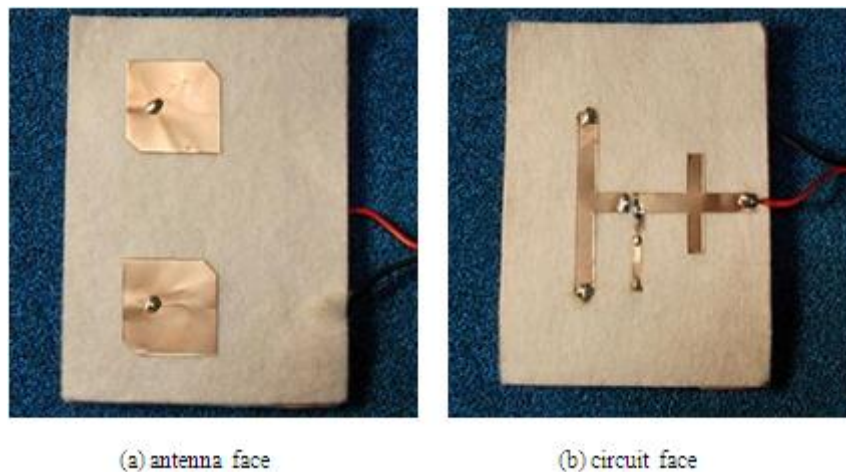


Figure 5.19 Picture of Rectenna with two antennas and one rectifier



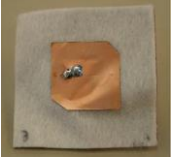
Table 5.8 Output Voltage of each rectenna

	1 antenna to 1 rectifier	2 antennas to 1 rectifier
Output Voltage [mV]	695	469

5.3.3 Comparison to the Conventional Rectennas

The light-weight flexible rectenna was compared with the conventional rectennas developed in our past study. Table 5.9 shows the result. It is found that the weight per unit area of the flexible patch was lighter than that of the conventional patch by above one order and the flexible patch was as thin as the thin membrane dipole. Therefore, the flexible patch is very attractive, considered mounting on the MAV model.

Table 5.9 Comparison of the some rectennas

Parameters	Conventional patch	Thin membrane dipole	Light-weight flexible patch
Weight [g]	10.675	0.65	1.6
Thickness [mm]	32	1	1.2
Weight per unit area [g/cm^2]	1.15	0.026	0.079
Polarized wave efficiency [%]	70	47	70
Picture			

5.4 MAV Model Demonstration

5.4.1 Parallel Connection of Rectenna

We can treat the rectenna elements as DC power supplies because the RF is converted to the DC by the diodes. Therefore, we can connect them each other in series and in parallel. The output voltage is increase with connecting them in series, and the output current does in parallel. By combining the method of the series connection and of the parallel one suitably according to the system, we can make the best use of the obtained power. We should prefer the parallel connection because of the report that the power combining loss with the parallel connections was smaller than with the series connection^[30].

The rectenna's optimized resistance was 100Ω . However, the internal resistance of the motor for the MAV model was 4Ω . Then 10 elements of the rectenna were arrayed in parallel to the motor as in Figure 5.20. Due to the parallel connection, the optimized resistance of each rectenna was reduced to 10Ω . In addition, the input power to the motor increased because of the parallel connection.

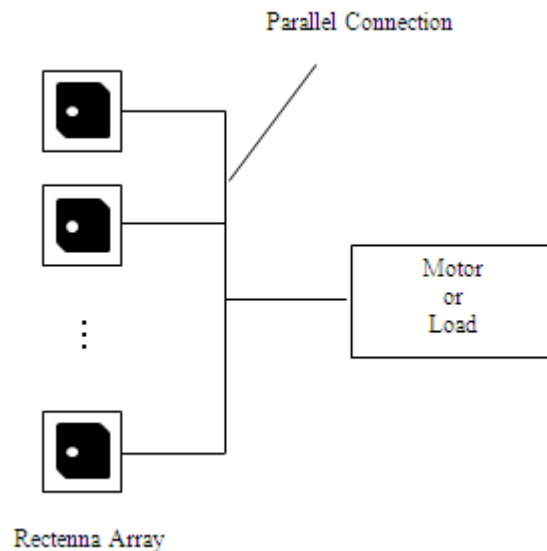


Figure 5.20 Schematic of Parallel Connection of Rectenna

5.4.2 Total Efficiency in Receiving System

The total efficiency in the receiving system is shown as a product of some efficiency of each component. Figure 5.21 shows the schematic of the receiving system. The total efficiency is expressed as:

$$\eta_{\text{receiving system}} = \eta_{\text{polarized wave}} \times \eta_{\text{return loss}} \times \eta_{\text{conversion}} \quad (5.4)$$

Although $\eta_{\text{polarized wave}}$ was average 0.7 and $\eta_{\text{return loss}}$ is 0.99, $\eta_{\text{conversion}}$ changes with the input power. Then, the total efficiency was calculated for the demonstration at 1500mm height from the horn antennas. At 1500mm height, since the rectenna could receive average 10mW RF power to the rectifier circuit (the input power to rectenna was 14.4mW) the conversion efficiency of the rectifier circuit was 28.1%. Therefore, the total efficiency in receiving system was calculated as 19.5%, $\eta_{\text{receiving system}} \sim 0.195$, and the DC power received by one rectenna was calculated as 2.81mW at 1500mm height from the transmission system.

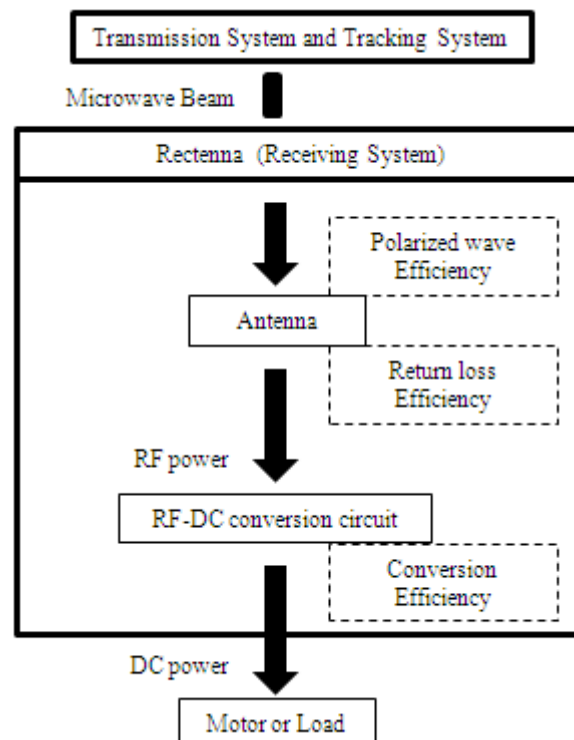


Figure 5.21 Schematic of Total Efficiency in Receiving System

5.4.3 MAV Model Demonstration

I tested the running the electric motor (4Ω load) and 10Ω load, and measured the output voltage and the DC power. Figure 5.22 shows the result when the MAV model circled 1500mm over the transmission system. The MAV position was tracked at all times by the tracking system and microwave beam was transmitted to the MAV at any time by the transmission system. As can be seen from the figure, the each rectenna element mounted on the MAV converted the microwave beam into average 1.8mW (at 10Ω load) or 1mW (at 4Ω load) DC power. Therefore, the MAV could receive average 18mW DC power (at 10Ω load) or 10mW DC power (at 4Ω load). This result is different from the calculated result discussed in previous section 5.4.2. It is assumed that the difference is caused by the tracking error. Because of this, the microwave beam power, in this experiment, was less than the power calculated.

However, the 18mW and 10mW DC power were enough to move the electric motor. Therefore, I succeeded to run the electric motor and demonstrate the MAV model mounting the Light-Weigh Flexible Rectennas.

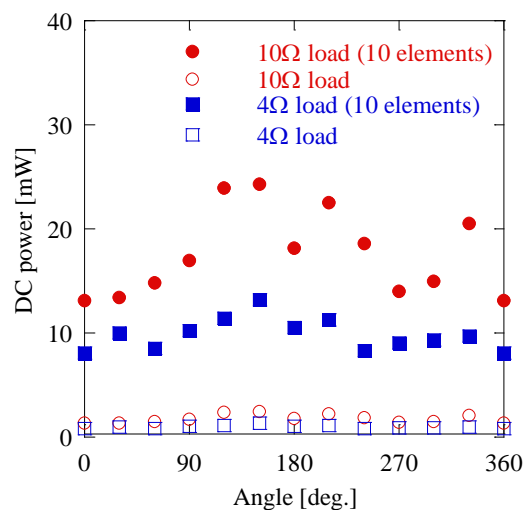


Figure 5.22 DC Power related to Angle

Chapter 6

Conclusions

This chapter shows the conclusions of my study, the perspectives and the issues in the future.

6.1 Conclusions

Some experimental studies on Light-Weight Flexible Rectenna in microwave wireless power transmission were conducted by the measurement of the efficiency and the properties. The conclusions are summarized as follows:

1. Light-Weight Flexible Rectennas were developed and it was found that the rectennas were not inferior to regular rectennas which were on hard dielectrics. In addition, in case of a mounting on a MAV, it is concluded that the light-weight flexible rectennas are very useful.
2. It was found that the antenna's polarized wave efficiency was average 70% related to the antenna's yaw angle.
3. It was seen that the antenna's return loss was about -20dB (efficiency was 99%) and the antenna efficiency of the rectennas declined 5% with 45-degree bend and 10% with 90-degree bend.
4. It was found that the conversion efficiency of the RF-DC conversion circuit was maximum 58% at 60mW RF power and 100 Ω load resistance, and the efficiency didn't decline with B-plane bend and declined with A-plane bend degrees.
5. It was concluded that the optimum array pitch of these rectennas was 0.85λ .
6. I demonstrated our MAV system and succeeded in driving the motor mounted on the MAV model.

6.2 Future Perspectives and Issues

The rectennas developed in this study have a possibility of improvement of the efficiency since it is felt that the polarized wave efficiency and the conversion efficiency has not been optimized yet. In addition, if a high quality Schottky Barrier diode is developed, the conversion efficiency surely becomes higher. Moreover, I designed the antennas by calculation based on the theory. However, I find there is still room for improvement in the position of the RF feeding point and the side length. In the future study, we should optimize the parameters with the analytical results from the computer simulations of the electromagnetic field, and actually confirm the improvement with the experiments.

In addition, though the small DC power was converted to in this experiment, the larger power will be converted to by combinations of the rectennas. Therefore, larger systems will be demonstrated and developed in the future than our MAV model system.

Finally, it was very difficult to mount rectennas on flying objects due to the rectenna's weight and hardness. However the light-weight flexible rectennas got over the problem, so it is expected that the rectennas are applied to many applications. Therefore, in our laboratory, we will apply them to spacesuits and so on, and develop new system in Microwave Wireless Power Transmission.

References

- [1] H. Kuwano: "Trends of Energy Harvesting Technologies," CMC Publishing Co., Ltd (2010)
- [2] H. Matsuki: "Frontier of Wireleses Electric Power Transmission," CMC Publishing Co., Ltd (2009)
- [3] A. Kurs, A. Karalis, R. Moffatt, J.D. Joannopoulos, P. Fisher, M. Soljacic: "Wireless Power Transfer via Strongly Coupled Magnetic Resonances," *Science*, **317**, pp. 83-86 (2007)
- [4] N. Kawashima: "Importance of the Development of a Rover for the Direct Confirmation of the Existence of Ice on the Moon," *Trans. Jap. Soc. Aeronaut. Space Sci.*, **43**, pp. 33-35 (2000)
- [5] 松本 紘, 篠原 真毅: "宇宙太陽光発電所とマイクロ波エネルギー伝送技術," *信学技報 SAT95-77*, **95**, 443, pp.31-36 (1995)
- [6] Brown W. C.: "A survey of the elements of power transmission by microwave beam," 1961 IRE Int. Convention Record **9**, 93-105 (1961)
- [7] Brown W. C.: "THE HISTORY OF WIRELESS POWER TRANSMISSION," *Solar Energy* Vol. **56**, No. 1 pp 3-21 (1996)
- [8] R. Ozawa, "Development of Microwave Energy Supply System," Master thesis, University of Tokyo (2007)
- [9] K. Katsunaga: "Developments of Polarity-Free Rectenna for Micro Aerial Vehicles," Master thesis, University of Tokyo (2007)
- [10] S. Komatsu., K. Katsunaga, R. Ozawa, K. Komurasaki and Y. Arakawa: "Power Transmission to a Micro Aerial Vehicle, AIAA paper 2007-**1003** (2007)
- [11] E. Shimane., S. Komatsu, K. Komurasaki and Y. Arakawa: "A MAV Flight using Microwave Power Supply," AIAA paper 2008-**1149** (2008)
- [12] D. Takahashi: "Development of light, flexible microwave receipt rectenna," Bachelor thesis, University of Tokyo (2008)

- [13] H. Sawahara, A. Oda, A. Diallo, K. Komurasaki, Y. Arakawa: "Power Beaming to a Micro Aerial Vehicle using an Active Phased Array," SPIE Smart Structures and Materials + Nondestructive Evaluation and Health Monitoring, SPIE7674, **76460S** (2010)
- [14] A. Oda, H. Sawahara, M. Ishiba, K. Komurasaki, Y. Arakawa: "Integration of MAV Wireless Power Transmission Systems," 8th Annual International Energy Conversion Engineering Conference, **771079** (2010)
- [15] M. Ishiba, A. Oda, H. Sawahara, K. Komurasaki, Y. Arakawa: "Wireless Communication and Power Transmission for a MAV flight," 2010 Asia-Pacific International Symposium on Aerospace Technology, **10YS429** (2009)
- [16] David M. Pozar: "Microwave Engineering second edition," Wiley (1997)
- [17] Robert S. Elliott: "Antenna Theory and Design Revised Edition," Wiley-IEEE Press (2003)
- [18] T. Yoo, K. Chang: "Theoretical and Experimental Development of 10 and 35 GHz rectennas," IEEE Trans. Microwave Theory and Tech., Vol.40, No.6 (1992)
- [19] 電子情報通信学会: "アンテナ工学ハンドブック," オーム社 (2001)
- [20] 羽石 操, 平澤 一紘, 鈴木 康夫: "小型・平面アンテナ," 電子情報通信学会 (1996)
- [21] 後藤 尚久: "アンテナ工学入門講座," 電波新聞社 (2008)
- [22] R. J. Gutmann and J. M. Borrego: "Power Combining in an Array of Microwave Power Rectifiers," IEEE Trans. Microwave Theory and Tech., Vol. MTT-27, pp. 958-968 (1979)
- [23] R. J. Gutmann and J. M. Borrego: "Solar power satellite rectenna design study: directional receiving elements and parallel-series combining analysis," NASA Final Rep. NAS9-15453, Ch. 3 (1978)
- [24] 谷口 慶治: "マイクロ波電子回路—設計の基礎—," 共立出版 (2004)
- [25] J. O. Mcspadden, T. Yoo and K. Chang: "Theoretical and Experimental Investigation of a Rectenna Element for Microwave Power Transmission," IEEE Trans. Microwave Theory and Tech., Vol. 40, pp. 2359-2366 (1992)
- [26] J. O. Mcspadden, L. Fan, K. Chang: "Design and Experiments of a High-Conversion-Efficiency 5.8GHz Rectenna," IEEE Trans. Microwave Theory and Tech., Vol. 46, pp. 2053-2060 (1998).
- [27] 田中 正人, 張 宰赫: "ウェアラブルパッチアンテナ," 信学技報 AP2002-76 (2002)
- [28] 山本 綱之, 藤森 和博, 佐藤 稔, 野木 茂次, 真田 篤志: "RF-DC 変換回路の変換効率に対するダイオードの接合容量の影響," 信学技報 WPT2010-11 (2010)
- [29] 篠原 真毅, 岡田 寛, 三谷 友彦, 松本 紘: "マイクロ波エネルギー伝送用レクテナ整流回路のパラメータ最適化に関する研究," 第 24 回宇宙エネルギーシンポジウム講演論文集 pp.125-129 (2005)
- [30] 三浦 健史, 篠原 真毅, 松本 紘: "マイクロ波電力伝送用レクテナ素子の接続法に関する実験的研究," 電子情報通信学会論文誌 B, Vol. J82-B, No.7, pp.1374-1383 (1999)

Accomplishments

Conference Presentations

学会発表

- [i] ○澤原弘憲, 小田章徳,, ディアロ・アルセニー, 小紫公也, 荒川義博
「MAV 用 5.8GHz レクテナの開発」
第 29 回宇宙エネルギーシンポジウム, 相模原, 2009 年 2 月

- [ii] *Sawahara H., Oda A., Diallo A., Komurasak K., Arakawa Y.
“Power Beaming to a Micro Aerial Vehicle using an Active Phased Array”
SPIE Smart Structures and Materials + Nondestructive Evaluation and Health Monitoring
SPIE7646, 76460S, San Diego, USA, March, 2010

- [iii] ○澤原弘憲, 小田章徳, 石場舞, 石田準, 小紫公也, 荒川義博, 田中孝治
「フレキシブルレクテナの開発」
第 54 回宇宙科学技術連合講演会, 1S15, 静岡, 2010 年 10 月

- [iv] ○澤原弘憲, 小田章徳, 石場舞, 小紫公也, 荒川義博, 田中孝治
「軽量フレキシブルレクテナ搭載 MAV へのマイクロ波自動追尾送電」
第 30 回宇宙エネルギーシンポジウム, 相模原, 2011 年 2 月

Conference Papers and Journals

学会誌掲載

- [a] 高橋大祐, ○澤原弘憲, 小田章徳, ディアロ・アルセニー, 小紫公也, 田中孝治, 藤野義之
「軽量フレキシブルレクテナ搭載マイクロ飛行機への無線電力伝送」
電気情報通信学 信学技報 SPS2009-04 (2009年7月)
- [b] ○澤原弘憲, 小田章徳,, ディアロ・アルセニー, 小紫公也, 荒川義博
「MAV用5.8GHzレクテナの開発」
第29回エネルギーシンポジウム 講演論文集 (2010年2月)
- [c] *Sawahara H., Oda A., Diallo A., Komurasak K., Arakawa Y.,
“Power Beaming to a Micro Aerial Vehicle using an Active Phased Array”
SPIE Smart Structures and Materials Internet Proceedings (2010年3月)
- [d] ○澤原弘憲, 小田章徳, 石場舞, 石田準, 小紫公也, 荒川義博, 田中孝治
「フレキシブルレクテナの開発」
第54回宇宙科学技術連合講演会 講演論文集 (2010年10月)
- [e] ○澤原弘憲, 小田章徳, 石場舞, 小紫公也, 荒川義博, 田中孝治
「軽量フレキシブルレクテナ搭載 MAV へのマイクロ波自動追尾送電」
第30回エネルギーシンポジウム 講演論文集 (2011年2月)
- [f] ○澤原弘憲, 小田章徳, 石場舞, 石田準, 勝永健太, 小澤亮二, 小松周平, 嶋根愛理, 高橋大祐, 小紫公也, 荒川義博, 田中孝治, 佐々木進
「軽量フレキシブルパッチレクテナの開発」
電気情報通信学会誌 (投稿中)